MODELS OF SLOW INTERGRANULAR VOID GROWTH

DUE TO VOID SURFACE AND GRAIN BOUNDARY SELF-DIFFUSION[*]

by

Keith Isamu Kagawa[†]

February 1976

† Formerly, Graduate Fellow and Research Assistant in Engineering, Brown
University. Current address: 2511-D Waiomao Road, Honolulu, Hawaii 96816.

* The text of this report is the author's M.Sc. thesis at Brown University:
the degree is to be awarded in June 1976.

MASTER

DISCLAIMER

This report was prepared as an account of work sponsored by an agency of the United States Government. Neither the United States Government nor any agency Thereof, nor any of their employees, makes any warranty, express or implied, or assumes any legal liability or responsibility for the accuracy, completeness, or usefulness of any information, apparatus, product, or process disclosed, or represents that its use would not infringe privately owned rights. Reference herein to any specific commercial product, process, or service by trade name, trademark, manufacturer, or otherwise does not necessarily constitute or imply its endorsement, recommendation, or favoring by the United States Government or any agency thereof. The views and opinions of authors expressed herein do not necessarily state or reflect those of the United States Government or any agency thereof.

DISCLAIMER

Portions of this document may be illegible in electronic image products. Images are produced from the best available original document.

Table of Contents

Acknowledgments

Abstract

of

Models of Slow Intergranular Void
Growth due to Void Surface and
Grain Boundary Self-Diffusion

by

Keith Isamu Kagawa
Brown University, 1976

Intergranular void growth at elevated temperature is studied here in cases for which the shape of the void is determined by void surface diffusion and growth occurs by diffusion from the void tip and along the grain boundary. Equations governing the void shape are linearized and this linearization shown not to lead to gross errors in light of the large differences in the reported values of diffusion coefficients. A similarity solution for void shape is derived, and assuming growth in a particular manner, the similarity shape is shown to be determined by the choice of $a^3 v/\Omega v^*$ where a is the void half-length, v is the speed of propagation of the void tip, Ω is the atomic volume, and v^* is a temperature dependent material parameter. An iterative solution for void shape which depends on $a^3 v/\Omega v^*$ is derived also.

By assuming the grain boundary flux to be distributed in such a manner that the grains separate as rigid bodies, the similarity and iterative shapes are linked to the applied stress, and the resulting growth models compared to the limiting cases of equilibrium and crack-like growth. The comparison indicates that void growth can be represented by a two-part solution where either the linearized equilibrium or the similarity model applies for small $a^3 v/\Omega v^*$, and the crack-like model applies for larger $a^3 v/\Omega v^*$.

An Appendix presents an analysis of relaxation times associated with a variety of diffusion mechanisms which are useful in determining the dominant mechanisms of matter transport.

1. Introduction

Structures and machine elements operated under conditions of high temperature and sustained loading often fail by excessive time-dependent deformation or the fracture that follows, even when the stresses involved are far below the "yield" stress of the material. In laboratory specimens tested under these conditions (temperature significantly above room temperature but below the melting temperature and tensile loading considerably below yield stress), voids have been observed to form preferentially on grain boundaries perpendicular to the tensile axis [1-3], suggesting that grain boundary void nucleation and growth play a major role in fracture at high temperature.

Sintering, the shrinking of existing voids at high temperature and under sustained compressive loading, is well known in powder metallurgy and is attributed to the diffusion of atoms by four main mechanisms: vapor evaporation and condensation, self-diffusion along free surfaces, self-diffusion along grain boundaries, and bulk diffusion through the lattice of the crystal. A general view is given by Ashby [4] who has made estimates of the contribution of each mechanism in relation to sintering in powder compacts.

It is reasonable to expect then, that the growth of voids through diffusion should play a major role in high-temperature fracture. Voids on the grain boundary can be nucleated at junctions of grains and at grain boundary-inclusion interfaces through an accumulation of vacancies. Once nucleated, these voids can grow by diffusion from the cavity tip and along the grain boundary, or by bulk diffusion from the surface of the void to the grain boundaries until the ligament is sufficiently reduced for fracture to occur.

Numerous studies of the growth of voids on a planar grain boundary perpendicular to the applied stress have been made. Hull and Rimmer [2] and Speight and Harris [5] estimated the time to rupture of a material with an array of spherical voids located on a planar grain boundary and in which atoms were transported from the surface of the cavity along the grain interface. A correction to the model was made by Weertman [6], who considered the appropriate boundary condition to be one of zero vacancy flux on the grain boundary at the midpoint between voids. Vitovec [7] then estimated the strain rate while taking into account the change in stress acting across the grain boundary due to changes in the ligament size.

Recently, Raj and Ashby [8] have done a study of void growth and nucleation taking into account grain boundary sliding.

All the above have assumed that surface diffusion is sufficiently active to assure that the voids retain shapes made up of spherical segments. This condition may not always hold and has led Chuang and Rice [9,10] to study the problem of a long, crack-like cavity located on a planar grain boundary whose shape and rate of growth (measured as tip velocity) are governed by the chemical potential at the surface and grain boundary. The grains themselves are assumed to be elastic and isotropic. The study indicates that below some critical growth velocity an adequate model of void growth can be constructed by assuming the grain boundary flux such that the grains separate as rigid bodies.

The present study examines 2-dimensional models of void growth that span the gap between the constant-curvature, Hull-Rimmer type of void and the long, crack-like cavity of Chuang and Rice. The material is considered to be isotropic and homogeneous and the continuum viewpoint will be maintained (lengths of interest are large compared to atomic dimensions). Voids are

assumed to have been nucleated and only their growth is studied here.

A similarity solution in which shape and velocity are determined by the choice of one parameter is obtained along with an iterative solution in which void shape is also a function of the same parameter. Both are compared to the constant-curvature and long, crack-like void shapes.

For a tensile load applied perpendicular to the grain boundary, the assumption of rigid grains is then shown to impose the conditions necessary for determination of the void shape and rate of growth through the chemical potential and atom flux evaluated at the void tip. The models are then compared to the Hull-Rimmer (H-R) type and Chuang-Rice (C-R) models of void growth.

Although only two-dimensional models are considered here, a similar analysis can be carried out for the axisymmetric case.

2. Discussion of the Chemical Potential

Diffusion analyses usually do not consider nonhomogeneous stress fields as contributing to the chemical potential for diffusion, and thus the driving force is often expressed in terms of concentrations of the diffusing species. But, for those problems in which significant stress fields are present, it is necessary to include fluxes due to the nonhomogeneous stress field and it becomes convenient to express the flux J as proportional to the gradient of the chemical potential of the species.

Consider a crystal at constant temperature T and subjected to a constant macroscopic pressure P_o. The atom flux due to self-diffusion is given by the expression

$$\underline{J} = - \frac{D}{\Omega kT} \underline{\nabla}\mu \tag{2.1}$$

where D is a diffusion coefficient, Ω is the atomic volume, k is Boltzmann's constant, and μ is the chemical potential defined as the work required to reversibly add an atom to the stressed crystal (as an interstitial or in a vacancy), and is referred to an unstressed reference crystal at T and P_o.

Stevens, Dutton, and Puls [11] have shown that assuming local equilibrium between vacancies, divacancies, and interstitials allows the driving potential μ to be expressed as

$$\mu = \mu_A - \mu_V \tag{2.2}$$

where μ_A is the chemical potential of an atom on a lattice site and μ_V is is the chemical potential of a vacancy.

To determine the chemical potential for self-diffusion, consider a very large crystal held rigidly at a large distance from its surface and with a

normal traction σ_n applied at the surface. The chemical potential at the interface is μ_A since the surface can be considered a sink for vacancies. Assuming the concentration of defects just below the surface to be in equilibrium with the surface allows the calculation of μ_A. It can be shown [12,13] that to the first order in stress,

$$\mu = \mu_o - \Omega\sigma_n - \left(\frac{1}{\rho_1} + \frac{1}{\rho_2}\right)\gamma_s\Omega \qquad (2.3)$$

where μ_o is the chemical potential of the reference crystal, ρ_1 and ρ_2 are the radii of curvature of the surface (with the center of curvature taken outside the crystal), and γ_s is the surface energy.

Assuming the concentration of defects to be constant with respect to time, conservation of mass dictates that within the crystal,

$$\underline{\nabla}\cdot\underline{J} = 0 , \qquad (2.4)$$

or combining eqns. (2.1) and (2.4),

$$\nabla^2\mu = 0 . \qquad (2.5)$$

If the value of μ can be determined at the boundaries of the crystal, the evaluation of the atom fluxes in the interior reduces to finding a solution to Laplace's equation with the appropriate boundary conditions given by eqn. (2.3)

Equation (2.3) will be used extensively in the following chapters to describe the chemical potential on the void surface and on the grain boundary.

3. The Shape of a Void on a Grain Boundary

Changes in the shape of a void located on a grain boundary can be accomplished by self-diffusion along the surface of the cavity, by bulk diffusion through the lattice, and by evaporation and condensation. It is expected that at temperatures significantly below the melting point of the material it should be more difficult to move an atom (or a vacancy) through the lattice than along a free surface, and thus lattice diffusion should be negligible compared to surface diffusion [14]. However, as the temperature approaches the melting point, lattice diffusion should contribute a significant part to the total atom flux.

In order to know the conditions under which surface diffusion is the dominant mechanism in determing the shape of the void, it is useful to compare the characteristic relaxation time of a free surface with periodic curvature when the atom flux is due to lattice diffusion and when it is due to surface diffusion. If τ_s , the characteristic time for surface diffusion, and τ_ℓ , the characteristic time for lattice diffusion, are such that $\tau_s/\tau_\ell < .1$, it can be expected that surface fluxes will be the more significant part of matter transport. Characteristic wavelengths for $\tau_s/\tau_\ell = .1$ of some common metals at $.5\ T_m$ and $.8\ T_m$ are given in Table I and are seen to be of the same order of magnitude as observed inter-void spacings, leading one to assume that lattice diffusion can usually be neglected in the determination of void shape. (See Appendix for a more complete discussion and the derivation of characteristic times.)

In a similar manner, the contribution to matter transport from surface diffusion and from evaporation-condensation can be compared. Table I gives the characteristic wavelengths for $\tau_s/\tau_v = .1$ of some common metals at

.5 T_m and .8 T_m , where τ_s and τ_v are the characteristic times for surface diffusion and evaporation-condensation respectively. Since the wavelengths are of the same order of magnitude as the observed inter-void spacing, surface diffusion can reasonably be assumed to be the dominant mechanism involved in determining the shape of voids.

The problem to be studied here is one of a void whose shape is altered by diffusion along its surface and in which matter is removed only from the void tip by grain boundary diffusion. In the hope of determining shapes between the extremes of the constant curvature and long, crack-like voids, a linearized governing equation is derived and two methods of solution are explored. The first leads to a similarity solution in which void shape is determined by fixing a dimensionless parameter and the second is an iterative scheme based on the constant curvature, equilibrium shape.

A short derivation of the limiting cases (corresponding to very slow and very rapid growth) will also be given to provide a basis for comparison and evaluation of the two solutions for void shape.

Expressions for curvature and flux at the void tip will also be derived and will be shown in the next section to be the link between the problem of determining the shape of the void and that of its growth due to an applied stress.

3.1. Derivation of the Linearized Governing Equation

For void spacings much smaller than the grain diameter, the grain can be modelled as a very large solid held rigidly at a distance from the surface that is large compared to the void length. The grain boundary void can be represented as a symmetric, cylindrical cavity on the surface of the solid described by $y(x,t)$ with the coordinate system fixed at the center of the void as in Figure 3.1.

The void tip angle ψ is assumed to be constant for all time and is determined by the usual surface energy considerations,

$$\cos \psi = \frac{\gamma_b}{2\gamma_s} \tag{3.1}$$

where γ_s and γ_b are the energies for a free surface and a grain boundary respectively.

Assuming the cavity shape to be governed only by surface diffusion significant to some depth δ_s (usually taken to be $\Omega^{1/3}$), the surface flux is given by

$$J_s = - \frac{D_s \delta_s}{\Omega kT} \frac{\partial \mu}{\partial s} \tag{3.2}$$

where J_s is the surface flux ($\frac{atoms}{m\ sec}$), D_s is the surface diffusion coefficient, and ∂s is an increment of length along the surface.

Conservation of mass requires

$$\frac{\partial J_s}{\partial s} = \frac{v_n}{\Omega} \tag{3.3}$$

where v_n is the normal velocity of the void surface, and, combining eqns. (3.2) and (3.3),

$$\frac{\partial^2 \mu}{\partial s^2} + \frac{v_n kT}{D_s \delta_s} = 0 \quad . \tag{3.4}$$

Since the void surface is traction free, and since $\kappa = - \frac{1}{\rho}$, eqn. (2.3) requires the chemical potential to be proportional to the curvature κ

$$\mu = \Omega \gamma_s \kappa \quad . \tag{3.5}$$

If the rate of change of void height is considered to be small, that is, $y' \ll 1$ (where the prime denotes differentiation with respect to x), the curvature can be expressed as

$$\kappa = y'' \ , \tag{3.6}$$

and from eqns. (3.4),(3.5), and (3.6), the governing equation can be written as

$$\frac{\partial^4 y}{\partial x^4} + \frac{1}{\mathscr{D}} \frac{\partial y}{\partial t} = 0 \ , \tag{3.7}$$

where $\mathscr{D} = \dfrac{D_s \gamma_s \delta_s \Omega}{kT}$. (In practice, y' is not small for most metals and this limitation is discussed later.)

Void symmetry requires that the slope and flux be zero at $x = 0$ ($y'(0,t) = 0$ and $y'''(0,t) = 0$) . The other two boundary conditions are obtained by specifying the void length and tip angle ($y(a,t) = 0$ and $y'(a,t) = - \psi$).

3.2. Limiting Cases

The limiting cases of constant curvature and long, crack-like shape are discussed here to facilitate later comparison with the similarity and iterative solutions. Both linearized and non-linearized solutions are given and compared for each limiting case.

3.2.1. Equilibrium Void Shape

If surface diffusion is much more active than grain boundary diffusion so that the void shape can be assumed to be one of constant curvature

$$\kappa = - \frac{\sin \psi}{a} \ , \tag{3.8}$$

the void shape is given by

$$y = \frac{a}{\sin \psi} \left[- \cos \psi + \sqrt{1 - \frac{x^2}{a^2} \sin^2 \psi} \ \right] \ . \tag{3.9}$$

The surface flux at the void tip $(J_s)_{tip}$ to be used later in coupling void shape to the rigid grain model, can be evaluated by relating the rate of

change of void volume to the flux at the tip to get

$$(J_s)_{tip} = \frac{av}{\Omega} \left[\frac{\psi}{\sin^2 \psi} - \cot \psi \right] \qquad (3.10)$$

where $v = \frac{da}{dt}$ is the tip velocity.

The case just discussed corresponds to very slow growth since the assumption of constant curvature implies that each point on the void surface is in equilibrium with every other point on the surface.

3.2.2. Linearized Equilibrium Void Shape

Under the linearization, constant curvature implies

$$y'' = \text{Constant} . \qquad (3.11)$$

After integration and evaluation of the constants, the linearized equilibrium void shape can be shown to be given by

$$y = \frac{\psi a}{2} \left[1 - \frac{x^2}{a^2} \right] , \qquad (3.12)$$

and the curvature by

$$\kappa = - \frac{\psi}{a} . \qquad (3.13)$$

Again, relating the rate of change of void volume to the flux at the tip gives

$$(J_s)_{tip} = \frac{2\psi av}{3\Omega} \qquad (3.14)$$

where the volume is evaluated by integrating the void shape of eqn. (3.12).

Since the curvature and flux at the tip are of primary importance in the void growth model, the error introduced in the linearization can be estimated by comparing the tip curvature and flux of the equilibrium and linearized equilibrium shapes for various tip angles. Figure 3.2 shows $-(\kappa)_{tip} a$ vs. ψ and Fig. 3.3 shows $[(J_s)_{tip} \Omega]/av$ vs. ψ. The linearized equilibrium shape

can be seen to give a reasonable representation of the equilibrium shape for smaller values of ψ with larger error as ψ approaches $\pi/2$.

3.2.3. Chuang-Rice Crack-like Shape

Consider a long, crack-like void such that it can be described as a semi-infinite cavity growing at constant velocity v . Chuang and Rice [9] have studied the shape of such a cavity without making the small angle linearization and have shown the curvature and flux at the void tip to be approximated well by the expressions

$$(\kappa)_{tip} = - \sqrt{2(1 - \cos\psi)} \left(\frac{v}{\mathscr{D}}\right)^{1/3} \qquad (3.15)$$

and

$$(J_s)_{tip} = \sqrt{2(1 - \cos\psi)} \frac{(\mathscr{D}v^2)^{1/3}}{\Omega} . \qquad (3.16)$$

This solution corresponds to the steady-state situation in which the void is growing so rapidly that matter is removed only from the tip of the void and the surface far away is not affected by the behavior of the tip region.

3.2.4. Linearized Crack-like Shape

A linearized form of the long, crack-like void can be derived as follows. Suppose the void can be modelled as a semi-infinite cavity growing at constant velocity v and that void shape is dependent only on the distance from the tip,

$$y(x,t) = g(\zeta) \qquad (3.17)$$

where $\zeta = x - a$ and $a = a_0 + vt$. Then,

$$\frac{\partial y}{\partial t} = - v \frac{dg}{d\zeta} \qquad (3.18)$$

and the linearized governing equation becomes

$$\frac{d^4 g}{d\zeta^4} - \frac{v}{\mathscr{D}} \frac{dg}{d\zeta} = 0 . \qquad (3.19)$$

The void shape is found to be

$$g(\zeta) = \psi \left(\frac{\mathcal{D}}{v}\right)^{1/3} \left\{1 - \exp\left[\left(\frac{v}{\mathcal{D}}\right)^{1/3}\zeta\right]\right\} . \tag{3.20}$$

From eqns. (3.6) and (3.20), the curvature at the void tip is

$$(\kappa)_{tip} = -\psi \left(\frac{v}{\mathcal{D}}\right)^{1/3} , \tag{3.21}$$

and from eqns. (3.2), (3.5), (3.6), and (3.20), the flux at the tip is

$$(J_s)_{tip} = \psi \frac{(\mathcal{D}v^2)^{1/3}}{\Omega} . \tag{3.22}$$

The error introduced in linearization can be estimated by examining the curves in Fig. 3.4 which represent plots of $-(\kappa)_{tip}\left(\frac{\mathcal{D}}{v}\right)^{1/3}$ or $\frac{(J_s)_{tip} \Omega}{(\mathcal{D}v^2)^{1/3}}$ vs ψ for the C-R and linearized crack-like shapes. The linearized shape is seen to be a good approximation to the C-R shape and together with the linearized equilibrium shape discussed earlier, will be useful in the evaluation of the similarity and iterative shapes yet to be derived.

3.3. Similarity Solution

An examination of the void profiles for the linearized equilibrium and crack-like voids given by eqns. (3.12) and (3.20) indicates the void shape to be independent of the physical dimensions of the void. Solutions having this property are known as similarity solutions which are obtained by substituting particular dimensionless variables into a partial differential equation, resulting in an ordinary differential equation only in terms of these dimensionless variables. Consider then, the pair of dimensionless variables

$$\xi = \frac{x}{(\mathcal{D}t)^{1/4}} \tag{3.23a}$$

and

$$\eta = \frac{y}{(\mathscr{D}t)^{1/4}} \tag{3.23b}$$

where η is a function of ξ only. Differentiation and substitution into eqn. (3.7) gives a fourth order linear ordinary differential equation in $\eta(\xi)$ and ξ ,

$$\frac{d^4\eta}{d\xi^4} - \frac{1}{4} \xi \frac{d\eta}{d\xi} + \frac{1}{4} \eta = 0 \ . \tag{3.24}$$

For a particular choice of $\xi_o = \frac{a}{(\mathscr{D}t)^{1/4}}$, the location of the void tip in dimensionless coordinates, the boundary conditions can be shown to be:
$\eta'(0) = 0$, $\eta'''(0) = 0$, $\eta(\xi_o) = 0$, and $\eta'(\xi_o) = -\psi$.

A power series solution of the form

$$\eta(\xi) = \sum_{n=0}^{\infty} A_n \xi^n \tag{3.25}$$

can be obtained where the coefficients are given by

$$A_{n+4} = A_n \frac{n-1}{4(n+1)(n+2)(n+3)(n+4)} \ . \tag{3.26}$$

Because of the symmetry conditions ($\eta'(0) = 0$ and $\eta'''(0) = 0$)), the coefficients of the odd power terms must be zero and η can be shown to be

$$\eta(\xi) = \psi B_o (1 - \frac{1}{96} \xi^4 - \frac{1}{215040} \xi^8 - \ . \ . \ .)$$

$$+ \psi B_2 (\xi^2 + \frac{1}{1440} \xi^6 + \frac{1}{5806080} \xi^{10} + \ . \ . \ .) \tag{3.27}$$

where B_o and B_2 are constants evaluated by fixing a ξ_o and solving subject to the tip conditions ($\eta(\xi_o) = 0$ and $\eta'(\xi_o) = -\psi$).

The void shape given in eqn. (3.27) is expressed in dimensionless quantities and hence is not dependent on the actual dimensions of the void but is determined by the choice of ξ_o .

If during growth of the void, the shape changes so that ξ_o can be taken to be a constant with respect to time, a relation for tip velocity can be obtained by differentiating eqn. (3.23a) to get

$$\xi_o^4 = 4 \left(\frac{a^3}{\Omega} \frac{v}{v^*} \right) \tag{3.28}$$

where v is the void tip velocity, $v = da/dt$, and $v^* = \mathscr{D}/\Omega = \gamma_s D_s \delta_s /kT$. Thus, the shape can be related to the dimensionless group $(a^3/\Omega)(v/v^*)$ and allows the comparison of the similarity solution with the linearized constant-curvature and long, crack-like limiting cases described earlier.

For very small choices of ξ_o, a good approximation to η can be made by neglecting all but the first two terms of eqn. (3.27), reducing the expression for η to the same form as eqn. (3.12). Thus, the similarity solution approaches that of the linearized equilibrium void when $(a^3/\Omega)(v/v^*)$ is chosen to be very small. The shapes predicted by the similarity solution for $\xi_o = 1, 2$ and 3 are compared to the linearized equilibrium shape in Fig. 3.5.

For somewhat larger choices of ξ_o, the power series truncated at 4 terms gives an adequate representation of the void shape and the solution becomes

$$\eta = A_o(1 - \frac{1}{96} \xi^4) + A_2(\xi^2 + \frac{1}{1440} \xi^6) \tag{3.29a}$$

where

$$A_o = \psi \xi_o (1 + \frac{1}{1440} \xi_o^4)/(2 + \frac{1}{40} \xi_o^4 - \frac{1}{69120} \xi_o^8) \tag{3.29b}$$

and

$$A_2 = - \psi(1 - \frac{1}{96} \xi_o^4)/\xi_o(2 + \frac{1}{40} \xi_o^4 - \frac{1}{69120} \xi_o^8) . \tag{3.29c}$$

It will be shown in a later section that the curvature and flux at the void tip are needed to couple the shape to the stress applied to the rigid

grain model. The curvature of the similarity solution can be obtained by taking derivatives of eqn. (3.27) with respect to ξ and the curvature at the void tip is

$$(\kappa)_{tip} = \frac{\psi \xi_o}{a} [B_o(- \frac{1}{8} \xi_o^2 - \frac{1}{3840} \xi_o^6 - \ldots)$$

$$+ B_2(2 + \frac{1}{48} \xi_o^4 + \frac{1}{64512} \xi_o^8 + \ldots)] . \tag{3.30}$$

From eqns. (3.2), 3.5), (3.6) and (3.27), the flux at the void tip is

$$(J_s)_{tip} = \frac{\psi \mathscr{D} \xi_o^2}{\Omega a^2} [B_o(- \frac{1}{4} \xi_o - \frac{1}{640} \xi_o^5 - \ldots)$$

$$+ B_2(\frac{1}{12} \xi_o^3 + \frac{1}{8064} \xi_o^7 + \ldots)] . \tag{3.31}$$

For large choices of ξ_o , numerical error associated with the evaluation of a sufficient number of terms to assure convergence of the power series necessitates a different scheme for the solution of eqn. (3.24). The ordinary differential equation and its associated boundary conditions make up a two point boundary value problem amenable to solution by methods known as two point shooting techniques [15]. Although more costly to evaluate than the series solution, the shooting technique is much more accurate for large choices of ξ_o .

If the similarity solution is a reasonable representation of void shape, it should approach the shape of the linearized, crack-like cavity given in eqn. (3.20) as ξ_o is chosen to be very large (fast growth). Figures 3.6a and 3.6b compare the shapes predicted by the similarity solution evaluated using a two point shooting technique to those of the linearized, crack-like cavity having the corresponding tip velocities given by eqn. (3.28). The shapes are not alike since choosing a ξ_o imposes an acceleration and higher

order time derivatives as well as a velocity. An examination of d^2a/dt^2 reveals a deceleration of the void tip, and it is both the deceleration and the high velocity associated with large choices of ξ_o that allow matter to be removed from the void tip to form a bulge.

However, it should be noted that the tip profiles of the similarity and the linearized, crack-like shapes are very much alike and that it is the tip parameters $(\kappa)_{tip}$ and $(J_s)_{tip}$ that will be of importance in the void growth models discussed later.

3.4. Iterative Solution

In the similarity solution the assumption that the rate of change of dimensionless void length, $d\xi_o/dt$, does not significantly contribute to the void tip velocity is made in order to incorporate velocity in the determination of void shape. A different approach can be adopted in which the velocity enters explicitly in the expression of void shape.

The governing partial differential equation as seen earlier is

$$\frac{\partial^4 y}{\partial x^4} = -\frac{1}{\mathscr{D}}\frac{\partial y}{\partial t} . \tag{3.32}$$

Assume that y can be represented by a series of functions,

$$y = y_o + y_1 + y_2 + \cdots , \tag{3.33}$$

where y_o is the linearized constant-curvature shape of eqn. (3.12) and y_n satisfies

$$\frac{\partial^4 y_{n+1}}{\partial x^4} = -\frac{1}{\mathscr{D}}\frac{\partial y_n}{\partial t} \tag{3.34}$$

for $n = 0, 1, 2, \cdots$

Since the boundary condition for slope at the void tip $(y'(a,t) = -\psi)$ is satisfied by y_o , the boundary conditions to be satisfied by the other y_n are: $y_n'(0,t) = 0$, $y_n'''(0,t) = 0$, $y_n(a,t) = 0$, and $y'_n(a,t) = 0$.

The first three such functions are:

$$y_o = \frac{\psi a}{2}\left[1 - \left(\frac{x}{a}\right)^2\right] , \tag{3.35}$$

$$y_1 = \frac{\psi a}{2}\left[-\frac{1}{360}\left(\frac{x}{a}\right)^6 - \frac{1}{24}\left(\frac{x}{a}\right)^4 + \frac{11}{120}\left(\frac{x}{a}\right)^2 - \frac{17}{360}\right]\left(\frac{a^3 v}{\Omega v^*}\right) , \tag{3.36}$$

and

$$
\begin{aligned}
y_2 = \frac{\psi a}{2}&\left[\frac{1}{1814400}\left(\frac{x}{a}\right)^{10} + \frac{45}{1814400}\left(\frac{x}{a}\right)^8 - \frac{462}{1814400}\left(\frac{x}{a}\right)^6\right.\\
&\left.+ \frac{3570}{1814400}\left(\frac{x}{a}\right)^4 - \frac{5939}{1814400}\left(\frac{x}{a}\right)^2 + \frac{2785}{1814400}\right]\frac{a^7}{\mathscr{D}^2}\frac{d^2 a}{dt^2}\\
+ \frac{\psi a}{2}&\left[-\frac{2}{1814400}\left(\frac{x}{a}\right)^{10} - \frac{924}{1814400}\left(\frac{x}{a}\right)^6 + \frac{14280}{1814400}\left(\frac{x}{a}\right)^4\right.\\
&\left.- \frac{25778}{1814400}\left(\frac{x}{a}\right)^2 + \frac{12424}{1814400}\right]\left(\frac{a^3 v}{\Omega v^*}\right)^2 .
\end{aligned}
\tag{3.37}
$$

As mentioned in the previous section, a disadvantage of the similarity solution is that it imposes a deceleration of the void tip. It is useful, then, to look at the iterative solution for constant velocity. The y_n for constant v can be straightforwardly obtained by computer and are shown in Fig. 3.7 for $a^3 v/\Omega v^* = 5$ and 1, 2, 3, 4, and 5 iterations. The shapes are seen to oscillate and an examination of the y_n suggests that for a sufficient number of iterations, the solution y oscillates infinitely for any value of $a^3 v/\Omega v^*$ chosen.

It now becomes necessary to determine under what consitions a reasonable estimate of void shape is given by the iterative solution. Since the iterative shape is dependent on the choice of $a^3 v/\Omega v^*$, $(a^7/\mathscr{D}^2)(d^2 a/dt^2)$, etc.,

which are the same dimensionless groups found in the similarity solution, one can compare the two. Figure 3.8 shows the similarity solution for $a^3 v/\Omega v^* = \xi_0^4/4 = 5$, 10, and 20 and the two iteration solution, $y = y_o + y_1 + y_2$ with the appropriate dimensionless velocity and acceleration groups. Good agreement between the two solutions gives some basis for using a two term iterative solution to represent a void growing at constant velocity for $a^3 v/\Omega v^* < 5$. These two iteration, constant velocity void shapes are shown in Fig. 3.9 for $a^3 v/\Omega v^* = 1$, 3, 5, and 10.

The curvature and surface flux necessary for coupling the void shape and the rigid grain model of the next section can be obtained from eqns. (3.2), (3.5), (3.6), (3.35), (3.36), and (3.37). Evaluation of the resulting expressions at the void tip for the two iteration solution gives

$$(\kappa)_{tip} = -\frac{\psi}{a} \left[1 + \frac{1}{5} \left(\frac{a^3 v}{\Omega v^*} \right) - \frac{359}{14175} \left(\frac{a^3 v}{\Omega v^*} \right)^2 \right.$$
$$\left. - \frac{77}{14175} \left(\frac{a^7}{\mathscr{D}^2} \frac{d^2 a}{dt^2} \right) \right] \tag{3.38}$$

and

$$(J_s)_{tip} = \frac{\psi \mathscr{D}}{\Omega a^2} \left[\frac{2}{3} \left(\frac{a^3 v}{\Omega v^*} \right) - \frac{4}{63} \left(\frac{a^3 v}{\Omega v^*} \right)^2 - \frac{4}{315} \left(\frac{a^7}{\mathscr{D}^2} \frac{d^2 a}{dt^2} \right) \right] . \tag{3.39}$$

3.5. Discussion

A viable model of void shape should predict growth in an equilibrium mode for velocities considered in some sense to be small and growth corresponding to the C-R model for larger velocities.

The linearized equilibrium, similarity, iterative, and linearized crack-like models of void shape are compared by plotting $-(\kappa)_{tip} a/\psi$ vs. $a^3 v/\Omega v^*$ in Fig. 3.10 and $(J_s)_{tip} \Omega a^2/\psi \mathscr{D}$ vs. $a^3 v/\Omega v^*$ in Fig. 3.11. Curves for the

constant velocity, two iteration model (eqns. (3.38) and (3.39), neglecting acceleration terms) are shown, as well as curves for the similarity solution (eqns. (3.30) and (3.31)) using the first 20 terms in the series solution for y .

The curves for the similarity solution are in good agreement with those of the linearized equilibrium model for small choices of $a^3 v/\Omega v^*$ and with the curves for the linearized crack-like model at larger values, indicating a smooth transition from the equilibrium mode to the steady state mode of void growth at approximately $a^3 v/\Omega v^* = 5$.

The curves for the two iteration model follow those for the linearized equilibrium shape closely but do not approach the behavior of the linearized crack-like model, leading one to expect that the iteration model is only useful in a limited range, $a^3 v/\Omega v^* \lesssim 5$.

As noted previously, both the similarity and iterative approaches to void shape are based on the assumption that $y' \ll 1$ (small angle). Table II shows the tip angles of common metals to range from 1.2 to 1.45 and thus the small angle assumption cannot be justified a priori. However, as demonstrated by the comparison of tip curvature and flux for the linearized and non-linearized limiting cases, the small angle assumption does not lead to gross errors, and since the experimentally determined values of D_s are often not even in order of magnitude agreement [16], it seems reasonable to make the small angle assumption in order to obtain a simple model of void shape.

Void shape has been shown to be determined by the choice of $a^3 v/\Omega v^*$ and in the next chapter the applied stress will be coupled to the shape through the curvature and surface flux evaluated at the void tip. It should be noted, however, that the shape predicted by the similarity solution assumes a particular manner of growth corresponding to ξ_o constant.

4. Rigid Grain Models of Void Growth

The growth of a void on a grain boundary is accomplished by removing matter from the void surface and transporting it to the grain boundary by diffusion through the grain or by diffusion from the void tip along the grain boundary. To determine the conditions under which one of the above is the dominant mechanism of matter transport, a comparison of characteristic times similar to that of the previous chapter can be made where the characteristic relaxation times are now for a periodic thickening at the grain interface. Characteristic wavelengths for $\tau_b/\tau_\ell = .1$ of some common metals at $.5\ T_m$ and $.8\ T_m$, where τ_b and τ_ℓ are the characteristic times due to grain boundary and lattice diffusion respectively, are given in Table I and are of the same order of magnitude as the observed void spacing. For this reason, lattice diffusion is neglected in the models considered here and only the flux along the grain interface is taken to account for the increase in volume of the void and the local grain boundary thickening δ. (See Appendix for the derivation of relaxation times and a more complete discussion.)

As mentioned earlier [10], for void tip velocities less than v_{cr} where

$$\frac{v_{cr}}{v^*} = 5.66 \left(\frac{D_s \delta_s}{D_b \delta_b}\right)^3 \left(\frac{\Omega^{1/3} E}{\gamma_s (1-\nu^2)}\right)^3 \qquad (4.1)$$

(E is Young's modulus, ν is Poisson's ratio, D_b is the grain boundary coefficient, and δ_b is the depth through which grain boundary diffusion is considered to act), a model of void growth can be constructed by assuming the grains to separate as rigid bodies, i.e., the grain boundary thickening δ is uniform along the grain interface.

In this section, the relation between applied stress and void growth for such a model will be explored. The applied stress will be found to determine the void shape through the flux and curvature of the void tip. The similarity and iterative shapes obtained earlier will be coupled to the rigid grain model and compared to the models utilizing the linearized equilibrium and linearized crack-like void shapes.

4.1. The Rigid Grain Assumption

In order to model the growth of voids on a grain boundary perpendicular to an applied stress, consider a very large crystal with a periodic array of symmetric, cylindrical voids with center to center spacing of 2b and located on a planar grain boundary as shown in Fig. 4.1. A uniform stress σ_∞ is applied at a distance large compared to 2b.

Conservation of mass requires

$$\frac{\partial J_b}{\partial x} + \frac{1}{\Omega} \frac{\partial \delta}{\partial t} = 0 \qquad (4.2)$$

where δ is the grain boundary thickening and J_b is the grain boundary flux given by

$$J_b = - \frac{D_b \delta_b}{\Omega kT} \frac{\partial \mu}{\partial x} . \qquad (4.3)$$

On the grain boundary, the significant part of the chemical potential is due to the normal stress transmitted across the grain interface, σ_n. Equations (2.3), 4.2), (4.3), and the fact that the rigid grain assumption implies that δ is not a function of x give

$$\frac{d^2 \sigma_n}{dx^2} = \text{Constant} . \qquad (4.4)$$

At the point midway between two voids, symmetry requires the flux to be zero, or from eqns. (2.3) and (4.3),

$$\sigma'_n(b - a) = 0 \qquad (4.5)$$

where the prime denotes differentiation with respect to x. The other two boundary conditions necessary for a solution of eqn. (4.4) are given by σ_o and σ'_o, the value of the stress and its derivative, respectively, evaluated at the void tip.

The resulting expression for σ_n is

$$\sigma_n(x) = \sigma_o + \sigma'_o(x - \frac{1}{2} \frac{x^2}{b-a}) \qquad (4.6)$$

and the applied stress is given by

$$\sigma_\infty = \frac{1}{b} \int_0^{b-a} \sigma_n(x)dx \qquad (4.7)$$

$$= \frac{b-a}{b} (\sigma_o + \frac{b-a}{3} \sigma'_o) . \qquad (4.8)$$

4.2. Void Growth Models

In order to obtain a complete model of void growth, the void profiles obtained earlier must be coupled to the rigid grain model of the previous section through the values of σ_o and σ'_o. From eqn. (2.3), equating the chemical potential of the surface and of the grain boundary at the void tip gives

$$\sigma_o = - \gamma_s(\kappa)_{tip} \qquad (4.9)$$

where κ is the curvature of the void.

Also, at the void tip, the surface fluxes must be equal to the grain boundary flux, or from eqns. (2.3) and (4.3)

$$2(J_s)_{tip} = \frac{D_b \delta_b}{kT} \sigma'_o \qquad (4.10)$$

where J_s is the surface flux.

The expressions for $(\kappa)_{tip}$ and $(J_s)_{tip}$ for the various models of void shape can now be used through eqns. (4.8), (4.9), and (4.10) to couple the shape to the applied stress. For the linearized equilibrium shape, eqns. (3.13), (3.14), and (4.8-4.10) give

$$\sigma_\infty = \psi\gamma_s \frac{b-a}{b}\left[\frac{1}{a} + \frac{4}{9}\frac{b-a}{a^2}\left(\frac{D_s\delta_s}{D_b\delta_b}\right)\left(\frac{a^3 v}{\Omega v^*}\right)\right] . \tag{4.11}$$

From eqns. (3.21), (3.22), and (4.8-4.10), the expression for the linearized crack-like shape is

$$\sigma_\infty = \psi\gamma_s \frac{b-a}{b}\left[\frac{1}{a}\left(\frac{a^3 v}{\Omega v^*}\right)^{1/3} + \frac{2}{3}\frac{b-a}{a^2}\left(\frac{D_s\delta_s}{D_b\delta_b}\right)\left(\frac{a^3 v}{\Omega v^*}\right)^{2/3}\right] \tag{4.12}$$

$(\kappa)_{tip}$ and $(J_s)_{tip}$ for the similarity solution are given by eqns. (3.31) and (3.32), respectively, but for a limited range of $a^3 v/\Omega v^*$ a four term solution for η may be used and from eqns. (3.28), (3.29a-c), (3.30), (3.31), and (4.8-4.10),

$$\sigma_\infty = \psi\gamma_s \frac{b-a}{b}\left\{\frac{1}{a}\left[2 + \frac{1}{2}\left(\frac{a^3 v}{\Omega v^*}\right) - \frac{1}{480}\left(\frac{a^3 v}{\Omega v^*}\right)^2\right]\right.$$

$$+ \frac{b-a}{a^2}\left(\frac{D_s\delta_s}{D_b\delta_b}\right)\left[\frac{8}{9}\left(\frac{a^3 v}{\Omega v^*}\right) - \frac{1}{135}\left(\frac{a^3 v}{\Omega v^*}\right)^2\right]\right\}$$

$$\Big/\left\{2 + \frac{1}{10}\left(\frac{a^3 v}{\Omega v^*}\right) - \frac{1}{4320}\left(\frac{a^3 v}{\Omega v^*}\right)^2\right\} . \tag{4.13}$$

The two iteration, constant velocity expression from eqns. (3.38), (3.39), and (4.8-4.10) is

$$\sigma_\infty = \psi\gamma_s \frac{b-a}{b} \left\{ \frac{1}{a} \left[1 + \frac{1}{5} \left(\frac{a^3 v}{\Omega v^*}\right) - \frac{359}{14175} \left(\frac{a^3 v}{\Omega v^*}\right)^2 \right] \right.$$

$$\left. + \frac{b-a}{a^2} \left(\frac{D_s \delta_s}{D_b \delta_b}\right) \left[\frac{2}{9} \left(\frac{a^3 v}{\Omega v^*}\right) - \frac{4}{189} \left(\frac{a^3 v}{\Omega v^*}\right)^2 \right] \right\} . \qquad (4.14)$$

4.3. Discussion

From a practical viewpoint, it is useful to know the void growth rate as a function of the applied stress, geometric parameters, and material proper-ties, but because of the nature of the similarity and iterative models of void shape an expression of growth rate valid for all velocities is diffi-cult to obtain. However, eqns. (4.13) and (4.14), the expressions for σ_∞ of the similarity model using only the first four terms of the series solu-tion for void shape and of the two iteration model respectively, can be expected to be valid over a limited range of $a^3 v/\Omega v^*$ and are easily inverted to obtain $b^3 v/\Omega v^*$ as a function of $D_s \delta_s / D_b \delta_b$, a/b , and $\sigma_\infty b/\psi\gamma_s$.

The linearized equilibrium, linearized crack-like, 4 term similarity, and constant velocity two iteration models are compared in Fig. 4.2 where $b^3 v/\Omega v^*$ is plotted against a/b for $D_s \delta_s / D_b \delta_b = 10$ and $\sigma_\infty b/\psi\gamma_s = 10$. The similarity and 2 iteration solutions agree with the linearized equilibrium model for small a/b (corresponding to small $a^3 v/\Omega v^*$) and predict a critical void size

$$\left(\frac{a}{b}\right)_{cr} = \left(1 + \frac{\sigma_\infty b}{\psi\gamma_s}\right)^{-1} \qquad (4.15)$$

below which void growth does not occur by diffusive mechanisms. Both solu-tions also approach the behavior of the linearized crack-like solution for larger a/b (corresponding to larger $a^3 v/\Omega v^*$) with the similarity solution

giving a smoother transition from equilibrium to crack-like growth, approaching the curve for the crack-like model at $a^3 v/\Omega v^* \approx 5$.

As discussed in a previous section, the similarity void shape used here has acceleration and higher order terms imposed when the velocity is fixed. However, due to the resemblance of the general behavior of the similarity and constant velocity, 2 iteration models of void growth for $a^3 v/\Omega v^* = 5$, the similarity expression can be used with some confidence over the limited range.

An adequate representation of void growth can be made by using the linearized equilibrium or the similarity model for $a^3 v/\Omega v^* \lesssim 5$ and the crack-like model for $a^3 v/\Omega v^* \gtrsim 5$. The linearized equilibrium model has the advantage of a simple expression for velocity in terms of applied stress, geometric parameters, and material properties, while the similarity model gives a smoother transition to the crack-like mode of growth.

The behavior of a two part model based on the similarity and crack-like models is shown in Figs. 4.3 and 4.4, where $b^3 v/\Omega v^*$ vs. a/b is plotted for various values of $D_s \delta_s/D_b \delta_b$ and $\sigma_\infty b/\psi \gamma_s$. As the applied stress is increased, the transition from equilibrium to crack-like growth should occur at lower values of a/b and is borne out by the curves in Fig. 4.3 where $D_s \delta_s/D_b \delta_b$ is held constant and $\sigma_\infty b/\psi \gamma_s$ is varied. Also, as $D_s \delta_s/D_b \delta_b$ becomes larger the void is expected to remain in an equilibrium growth mode for larger velocities and the transition region is expected to occur at larger values of a/b . This trend is shown in Fig. 4.4 where $\sigma_\infty b/\psi \gamma_s$ is held constant as $D_s \delta_s/D_b \delta_b$ is varied. Thus, the 2 part model exhibits the behavior necessary for an adequate model of void growth.

5. Conclusion

Two dimensional models of grain boundary void growth have been discussed. Void shape has been assumed to be determined by surface diffusion and the change of void volume has been assumed to be accomplished by diffusion from the void tip and along the grain boundary. Equations governing the void shape have been linearized and the linearization shown not to be a particularly restrictive assumption. Assuming a particular mode of growth, a similarity solution has been obtained in which the void shape is determined by the choice of $a^3v/\Omega v^*$. An iterative solution whose shape is dependent on $a^3v/\Omega v^*$ has been derived also.

Assuming rigid grains, the similarity and iterative solutions have been coupled to the applied stress through the curvature and surface flux at the void tip. While the determination of the stress necessary for void growth at a given velocity can be obtained straightforwardly, the inverse problem of determining void growth when the applied stress is known is not as easily solved and, finally, void growth has been described by a two part solution in which either the linearized equilibrium or an approximation to the similarity solution is used for $a^3v/\Omega v^* \leq 5$, and the crack-like model is used for $a^3v/\Omega v^* \geq 5$. The two part model has been shown to exhibit the behavior expected of a reasonable model of void growth: a minimum void size for diffusive growth as well as growth in an equilibrium mode at low velocities and growth in a steady-state, crack-like mode at larger velocities.

It should be noted that under conditions of large applied stress and low $D_s\delta_s/D_b\delta_b$, estimates of time to rupture based on this model may differ from those obtained using Hull-Rimmer type models and these differences should be explored as well as void nucleation and the eventual rupture of the material due to plastic flow in the ligaments.

References

[1] Greenwood, J. N., Miller, D. R., and Suiter, J. W., Acta Met. **2**, 250, (1954).

[2] Hull, D., and Rimmer, D. E., Phil. Mag. **4**, 673, (1959).

[3] Fleck, R. G., Taplin, D. M. R., and Beevers, C. J., Acta Met. **23**, 415, (1975).

[4] Ashby, M. F., Acta Met. **22**, 275, (1974).

[5] Speight, M. V., and Harris, J. E., Metal Sci. J. **1**, 83, (1967).

[6] Weertman, J., Scripta Met. **7**, 1129, (1973).

[7] Vitovec, F. H., J. Mat. Sci. **7**, 615, (1972).

[8] Raj, R., and Ashby, M. F., Acta Met. **23**, 653, (1975).

[9] Chuang, T.-j., and Rice, J. R., Acta Met. **21**, 1625, (1973).

[10] Chuang, T.-j., Ph.D. Thesis at Brown University, (1974).

[11] Stevens, R. N., Dutton, R., and Puls, M. P., Acta Met. **22**, 629, (1974).

[12] Herring, C., J. Appl. Phys. **21**, 437, (1950).

[13] Herring, C., chapter in "The Physics of Powder Metallurgy," ed. W. E. Kingston, McGraw-Hill, (1951).

[14] Shewmon, P. G., "Diffusion in Solids," McGraw-Hill, (1963).

[15] Roberts, S. M., and Shipman, J. S., "Two Point Boundary Value Problems: Shooting Method," American Elsevier, (1972).

[16] Neumann, G., and Neumann, G. M., "Surface Self-Diffusion of Metals," Diffusion Information Center, (1972).

[17] Mullins, W. W., J. Appl. Phys. **30**, 77, (1959).

[18] Kennard, E. H., "Kinetic Theory of Gases," McGraw-Hill, (1938).

[19] Fung, Y. C., "Foundations of Solid Mechanics," Prentice-Hall, (1965).

Appendix: Characteristic Relaxation Times

In order to determine the conditions under which self-diffusion along the surface of the void and along the grain boundary are the only significant mechanisms of matter transport, it is useful to compare the characteristic relaxation time for each mode of transport due to a periodic disturbance. Mullins [17] has derived characteristic times for a periodic curvature on a free surface in the two dimensional case and the extension to three dimensions is given here. The characteristic times for a periodic grain boundary thickening, modelled by a periodic normal stress on a free surface, are also derived here.

A.1. The Free Surface

Consider a semi-infinite, isotropic solid occupying the half space $z \geq w$, where w is a free surface given by

$$w(x,y,t) = A(t) \exp \left[i \, \frac{2\pi x}{\ell} \right] \exp \left[i \, \frac{2\pi y}{L} \right] . \tag{A1}$$

$A(t)$ is taken to be much smaller than both ℓ and L .

From eqn. (2.3), the chemical potential on a free surface is proportional to the curvature and is

$$(\mu)_{surface} = \mu_o - \Omega \gamma_s \, c^2 \, w(x,y,t) \tag{A2}$$

where

$$c = \left[\left(\frac{2\pi}{\ell} \right)^2 + \left(\frac{2\pi}{L} \right)^2 \right]^{1/2} . \tag{A3}$$

A.1.1. Relaxation Due to Surface Self-Diffusion

If only surface diffusion is considered active, and then only through some depth from the surface δ_s (usually taken to be $\Omega^{1/3}$), conservation of mass requires

$$\frac{\partial (J_s)_x}{\partial x} + \frac{\partial (J_s)_y}{\partial y} = \frac{1}{\Omega} \frac{\partial w}{\partial t} \qquad (A4)$$

where $(J_s)_x$ and $(J_s)_y$ are surface fluxes in the x and y directions respectively. Substitution of eqn. (3.2) and eqn. (A1) gives

$$A'(t) + \frac{\Omega \gamma_s D_s \delta_s c^4}{kT} A(t) = 0 , \qquad (A5)$$

and the relaxation time is

$$\tau_s = \frac{kT}{\Omega \gamma_s D_s \delta_s} \left[\left(\frac{2\pi}{\ell} \right)^2 + \left(\frac{2\pi}{L} \right)^2 \right]^{-2} . \qquad (A6)$$

A.1.2. Relaxation Due to Lattice Self-Diffusion

For the case in which only lattice diffusion is active, an estimate of the relaxation time can be made by assuming the concentration of defects to be time independent. Then, continuity requires that the chemical potential satisfy Laplace's equation.

It is reasonable to expect that the magnitude of the atom flux tends to zero at large distances from the surface, leading to the condition that μ is equal to a constant as $z \to \infty$. The expression for μ at the surface is given by eqn. (A2) and the determination of the atom flux throughout the solid reduces to the problem of finding the solution to Laplace's equation, given the boundary conditions outlined above. The expression for μ is

$$\mu = \mu_o - \Omega \gamma_s c^2 \exp [-cz] w(x,y,t) . \qquad (A7)$$

Conservation of mass at the surface requires

$$\frac{1}{\Omega} \frac{\partial w}{\partial t} = (J)_z \qquad (A8)$$

where $(J)_z$ is the flux in the z direction, given by

$$(J)_z = - \frac{D_\ell}{\Omega kT} \frac{\partial \mu}{\partial z} . \qquad (A9)$$

Substitution of eqns. (A1), (A7), and (A9) into eqn. (A8) results in an ordinary differential equation in $A(t)$ with a characteristic time

$$\tau_\ell = \frac{kT}{\Omega \gamma_s D_\ell} \left[\left(\frac{2\pi}{\ell}\right)^2 + \left(\frac{2\pi}{L}\right)^2 \right]^{-3/2} . \tag{A10}$$

A.1.3. Relaxation Due to Evaporation-Condensation

Consider the surface to be in equilibrium with its own vapor at pressure P. Assuming the vapor to be a perfect gas, P can be found by equating the chemical potential of the solid and of the vapor at the surface, with both referred to a common reference crystal, and is given by

$$\ln \left(\frac{P}{P_o}\right) = \kappa \frac{\gamma_s \Omega}{kT} \tag{A11}$$

where P_o is the vapor pressure over a flat reference crystal and κ is the curvature of the surface under consideration.

From kinetic theory [18] the flux from the surface can be approximated by

$$\Theta - \Theta_o = \frac{\Delta P}{(2\pi mkT)^{1/2}} \tag{A12}$$

where Θ_o is the rate of evaporation from a flat surface, $\Delta P = P - P_o$, and m is the mass of a molecule of the material.

A mass balance at the surface requires

$$\frac{\Delta P}{(2\pi mkT)^{1/2}} = \frac{1}{\Omega} \frac{\partial w}{\partial t} . \tag{A13}$$

For ΔP small,

$$\frac{\Delta P}{P_o} \approx \kappa \frac{\gamma_s \Omega}{kT} , \tag{A14}$$

and substituting eqn. (A1) and (A14) into (A13) results in a first order,

linear ordinary differential equation in $A(t)$ with a characteristic time

$$\tau_v = \frac{(2\pi m)^{1/2}(kT)^{3/2}}{P_o \Omega^2 \gamma_s} \left[\left(\frac{2\pi}{\ell}\right)^2 + \left(\frac{2\pi}{L}\right)^2 \right]^{-1} \quad . \tag{A15}$$

A.2. The Grain Boundary

Consider a local grain boundary thickening δ and its associated normal stress distribution on the grain interface σ_n produced by placing matter selectively on the grain boundary.

The grain interface can be modelled as the surface of a semi-infinite solid occupying $z \geq 0$. If the solid is isotropic and linear elastic and the stresses at the surface are of the form

$$\sigma_n = \sigma_{zz} = B(t) \exp\left[i \frac{2\pi x}{\ell}\right] \exp\left[i \frac{2\pi y}{L}\right] \tag{A16a}$$

and

$$\sigma_{yz} = \sigma_{xz} = 0 , \tag{A16b}$$

the linear elasticity solution [19] gives a grain boundary thickening

$$\delta = - \frac{2(1-\nu)}{Gc} \sigma_n \tag{A17}$$

where

$$c = \left[\left(\frac{2\pi}{\ell}\right)^2 + \left(\frac{2\pi}{L}\right)^2 \right]^{1/2} \tag{A18}$$

and $\frac{1-\nu}{G} B(t)$ is much smaller than 1 .

From eqns. (2.3) and (A16a), the expression for chemical potential on the surface is

$$(\mu)_{surface} = \mu_o - \Omega\sigma_n \quad . \tag{A19}$$

A.2.1. Relaxation Due to Grain Boundary Self-Diffusion

If only grain boundary diffusion is assumed to be active, conservation of mass at the interface requires

$$\frac{\partial (J_b)_x}{\partial x} + \frac{\partial (J_b)_y}{\partial y} + \frac{1}{\Omega} \frac{\partial \delta}{\partial t} = 0 \ . \tag{A20}$$

Substitution of eqns. (4.3), (A16a), (A17), and (A19) into (A20) results in
a first order linear ordinary differential equation in $B(t)$ with character-
istic time

$$\tau_b = \frac{2(1-\nu)}{G} \frac{kT}{D_b \delta_b \Omega} \left[\left(\frac{2\pi}{\ell}\right)^2 + \left(\frac{2\pi}{L}\right)^2 \right]^{-3/2} \ . \tag{A21}$$

A.2.2. Relaxation Due to Lattice Self-Diffusion

Now, assume bulk diffusion and neglect diffusion along the grain boundary.
If the concentration of defects is time independent, conservation of mass re-
quires that the chemical potential satisfy Laplace's equation in the material.
Again, it is reasonable to expect that the magnitude of the flux tends to
zero at distances from the grain boundary that are large compared to ℓ and
L . The expression for μ at the boundary interface is given by eqns. (A16)
and (A19) and the determination of the flux throughout the solid then reduces
to the solution of Laplace's equation subject to the appropriate boundary con-
ditions. The expression for μ is

$$\mu = \mu_o - \Omega \sigma_n \exp \left[- cz\right] \ . \tag{A22}$$

Conservation of mass at the interface gives

$$\frac{1}{2\Omega} \frac{\partial \delta}{\partial t} + (J)_z = 0 \ . \tag{A23}$$

Substitution of eqns. (4.3), (A16a), (A17), and (A19) into (A23) results in
a first order linear ordinary differential equation in $B(t)$ with character-
istic relaxation time

$$\tau_\ell = \frac{1-\nu}{G} \frac{kT}{D_\ell \Omega} \left[\left(\frac{2\pi}{\ell}\right)^2 + \left(\frac{2\pi}{L}\right)^2 \right]^{-1} \ . \tag{A24}$$

A.3. Remarks

An estimate of the contribution to the total atom flux on a free surface due to surface self-diffusion, lattice diffusion, and evaporation-condensation can be made by examining the ratios of the characteristic relaxation times for each mechanism. In the two-dimensional case, taking ℓ or L tending to infinity, eqns. (A6) and (A10) give

$$\frac{\tau_s}{\tau_\ell} = \frac{D_\ell}{D_s \delta_s} \frac{\lambda}{2\pi} \tag{A25}$$

and eqns. (A6) and (A15) give

$$\frac{\tau_s}{\tau_v} = \frac{P_o \Omega}{D_s \delta_s (2\pi m k T)^{1/2}} \left(\frac{\lambda}{2\pi}\right)^2 . \tag{A26}$$

If $\tau_s/\tau_\ell \ll 1$ and $\tau_s/\tau_v \ll 1$ for a given λ, surface diffusion can be expected to be the dominant mechanism of matter transport for free surface disturbances of wavelength less than λ.

In a similar manner, a comparison of grain boundary diffusion and lattice diffusion can be made. For the two dimensional case, from eqns. (A21) and (A24),

$$\frac{\tau_b}{\tau_\ell} = \frac{D_\ell}{D_b \delta_b} \frac{\lambda}{\pi} \tag{A27}$$

and, if $\tau_b/\tau_\ell \ll 1$ for a given λ, grain boundary diffusion can be expected to be dominant for matter transport near grain boundary disturbances of wavelength less than λ.

The diffusion coefficients are found to obey an empirical law of the form

$$D = D_o \exp \left[-\frac{Q}{RT}\right] \tag{A28}$$

where D_o is a constant known as the frequency factor, R is the universal gas constant, Q is an activation energy, and T is the absolute temperature.

Representative values of the diffusion coefficients for some metals are given in Table I as well as values for λ_{max} , the characteristic wavelength for the ratios of characteristic time equal to .1, at .5 T_m and .8 T_m.

In practice, there are large discrepancies in the reported values of the coefficients and activation energies for surface and grain boundary diffusion and are usually attributed to difficulties in measurement of appropriate parameters and impurity effects.

Table I. Material properties and λ_{max} for $\tau_s/\tau_\ell = .1$, $\tau_s/\tau_v = .1$,
and $\tau_b/\tau_\ell = .1$ at $T = .5 T_m$ and $T = .8 T_m$.

	Cu	Ag	Zn	αFe	γFe	Ni
$T_m(K)^{(1)}$	1356	1234	694	1809	1809	1723
$\Omega(m^3) \times 10^{29(3)}$	1.18	1.71	1.52	1.18	1.18	1.10
Atomic weight (kg/kmol)[1]	63.54	107.87	65.37	55.85	55.85	58.71
$D_{so}(m^2/sec)^{(2)}$	2.0	.25	9.4×10^{-6}	10.	.4	4.2×10^{-2}
Q_s(kcal/mol)	49.0	41.6	6.17	55.6	49.0	47.7
$D_{bo}(m^2/sec)^{(1)(a)}$		1.2×10^{-5}	2.2×10^{-5}	2.5×10^{-4}	3.4×10^{-4}	1.75×10^{-4}
Q_b(kcal/mol)		21.5	14.3	40.0	39.0	28.2
$D_{\ell o}(m^2/sec)^{(1)}$	3.3×10^{-5}	4.9×10^{-5}	3.55×10^{-5}	1.9×10^{-4}	1.8×10^{-5}	2.59×10^{-4}
Q_ℓ(kcal/mol)	48.3	44.5	23.0	57.2	64.5	69.5
At $T = .5 T_m$						
$D_s\delta_s/D_b\delta_b$		8.1×10^{-4}	2.8×10^2	3.1	2.0	1.2×10^{-3}
$P_o(P_a)^{(1)}$	3.8×10^{-6}	5.3×10^{-6}	2.6×10^{-3}	10^{-7}	10^{-7}	7.4×10^{-7}
$\lambda_{max}(\mu m)^{(b)}$ (for $\tau_s/\tau_\ell = .1$	5.1	8.8	1.7×10^4	18.	1.8×10^4	7.7×10^3
$\lambda_{max}(\mu m)$ (for $\tau_s/\tau_v = .1$)	1.0	.98	5.8	2.2×10^2	2.8×10^2	26.
$\lambda_{max}(\mu m)$ (for $\tau_b/\tau_\ell = .1$)		5.5×10^3	30.	3.0	4.3×10^3	3.2×10^6

Table I. (Continued)

	Cu	Ag	Zn	αFe	γFe	Ni
At $T = .8\ T_m$						
$D_s \delta_s / D_b \delta_b$		.38	3.4	80.	17.	8.5×10^{-2}
$P_o(P_a)^{(1)}$	6.2×10^{-2}	2.9×10^{-2}	4.1	2.3×10^{-4}	2.3×10^{-4}	8.5×10^{-3}
$\lambda_{max}(\mu m)^{(b)}$ (for $\tau_s/\tau_\ell = .1$)	6.3	3.6	1.8	13.	7.0×10^2	65.
$\lambda_{max}(\mu m)$ (for $\tau_s/\tau_v = .1$)	8.4	8.7	.89	1.7×10^3	1.1×10^3	51.
$\lambda_{max}(\mu m)$ (for $\tau_b/\tau_\ell = .1$)		4.8	.26	8.2×10^{-2}	21.	3.8×10^2

References: (1) Smithells, C. J., "Metals Reference Book," 4th ed., Butterworth (1967).

(2) Neumann, G., and Neumann, G. M., "Surface Self-Diffusion of Metals," Diffusion Information Center (1972).

(3) "Handbook of Materials Science," ed. C. T. Lynch, CRC Press (1974).

(a) Values for $\delta_b = 5 \times 10^{-4}$ μm .

(b) Calculated assuming $\delta_s = \Omega^{1/3}$.

Table II. Values of γ_g, γ_s, and ψ for some metals.

Material	$\gamma_g (\frac{ergs}{cm^2})$	$\gamma_s (\frac{ergs}{cm^2})$	$\psi = \cos^{-1} \frac{\gamma_g}{2\gamma_s}$
Ag	790	1140	1.22
Au	364	1485	1.45
Cu	646	1725	1.38
Fe	780	1950	1.37
Ni	690	1725	1.37
Pt	1000	3000	1.40

Data from P. J. Hirth and J. Lothe, "Theory of Dislocations," McGraw-Hill (1968).

Figure Captions

3.1. Coordinate system for void shape.

3.2. Comparison of $-(\kappa)_{tip}a$ for equilibrium and linearized equilibrium void shapes for various tip angles.

3.3. Comparison of $(J_s)_{tip}\Omega/av$ for equilibrium and linearized equilibrium void shapes for various tip angles.

3.4. Comparison of $-(\kappa)_{tip}(\mathscr{D}/v)^{1/3}$ or $(J_s)_{tip}\Omega/(\mathscr{D}v^2)^{1/3}$ for the Chuang-Rice and linearized crack-like void shapes for various tip angles.

3.5. Void shapes predicted by the similarity solution for $\xi_o = 1, 2,$ and 3.

3.6. Comparison of void shapes predicted by the similarity and linearized crack-like solutions for (a) $\xi_o = 8$ and (b) $\xi_o = 16$.

3.7. Void shapes predicted by the iterative solution for constant velocity, v, where $(a^3v/\Omega v^*) = 5$.

3.8. Comparison of the two iteration and similarity void shapes for $(a^3v/\Omega v^*) = 5, 10,$ and 20.

3.9. Void shapes predicted by the two iteration solution for constant velocity v where $(a^3v/\Omega v^*) = 1, 3, 5,$ and 10.

3.10. Plots of $(\kappa)_{tip}(a/\psi)$ vs. $(a^3v/\Omega v^*)$ for the linearized equilibrium, similarity, constant velocity two iteration, and linearized crack-like void shapes.

3.11. Plots of $(J_s)_{tip}(\Omega a^2/\psi\mathscr{D})$ vs. $(a^3v/\Omega v^*)$ for the linearized equilibrium, similarity, constant velocity two iteration, and linearized crack-like void shapes.

4.1. Coordinate system for the rigid grain model.

4.2. Void growth models using the linearized equilibrium, 4 term similarity, constant velocity two iteration, and linearized crack-like void shapes for $(D_s\delta_s/D_b\delta_b) = 10$ and $(\sigma_\infty b/\psi\gamma_s) = 10$.

4.3. Void growth using a 2 part solution (4 term similarity and linearized crack-like) for $(D_s \delta_s / D_b \delta_b) = 10$ and $(\sigma_{\infty b} / \psi \gamma_s) =$ (a) 1, (b) 10, and (c) 20 . The dashed line indicates transition at $(a^3 v / \Omega v^*) = 5$.

4.4. Void growth using a 2 part solution (4 term similarity and linearized crack-like) for $(\sigma_{\infty b} / \psi \gamma_s) = 10$ and $(D_s \delta_s / D_b \delta_b) =$ (a) 2, (b) 10, and (c) 100 . The dashed line indicates transition at $(a^3 v / \Omega v^*) = 5$.
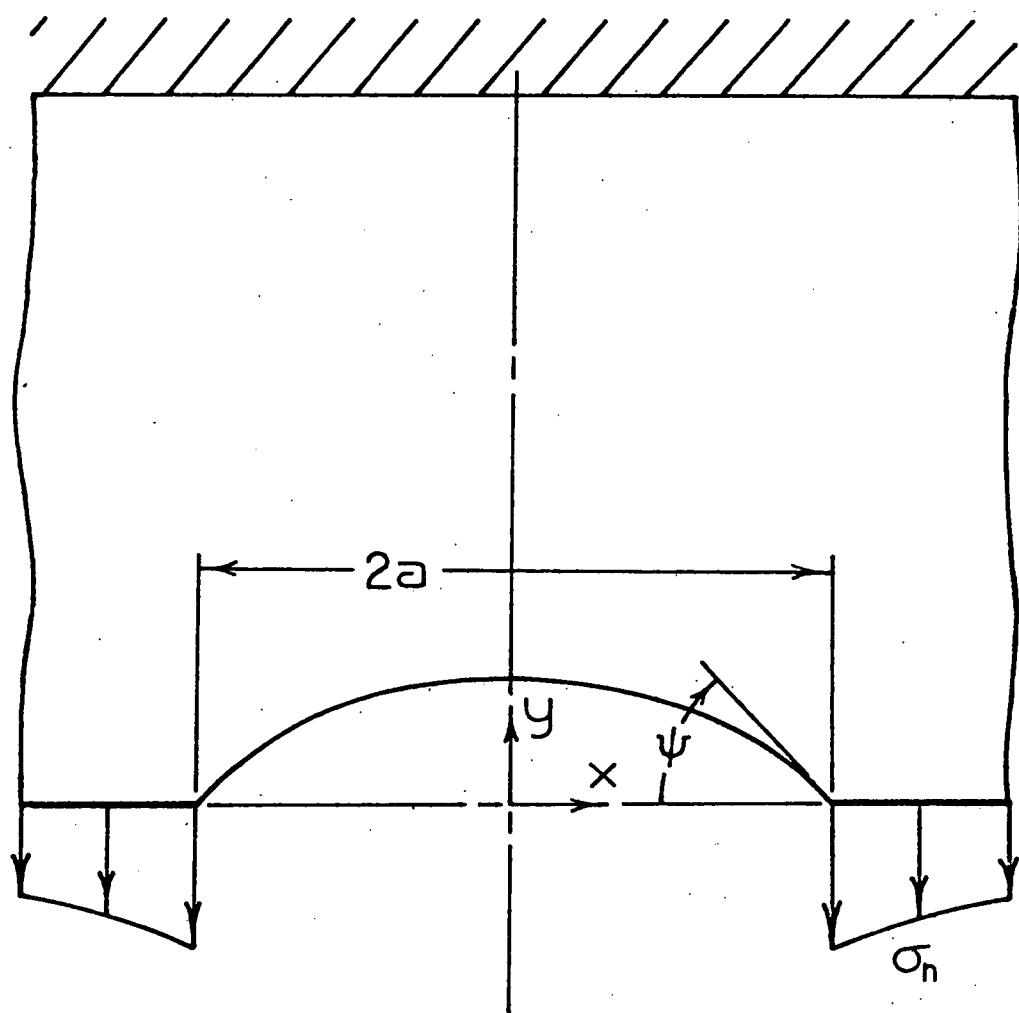
FIGURE 3.1
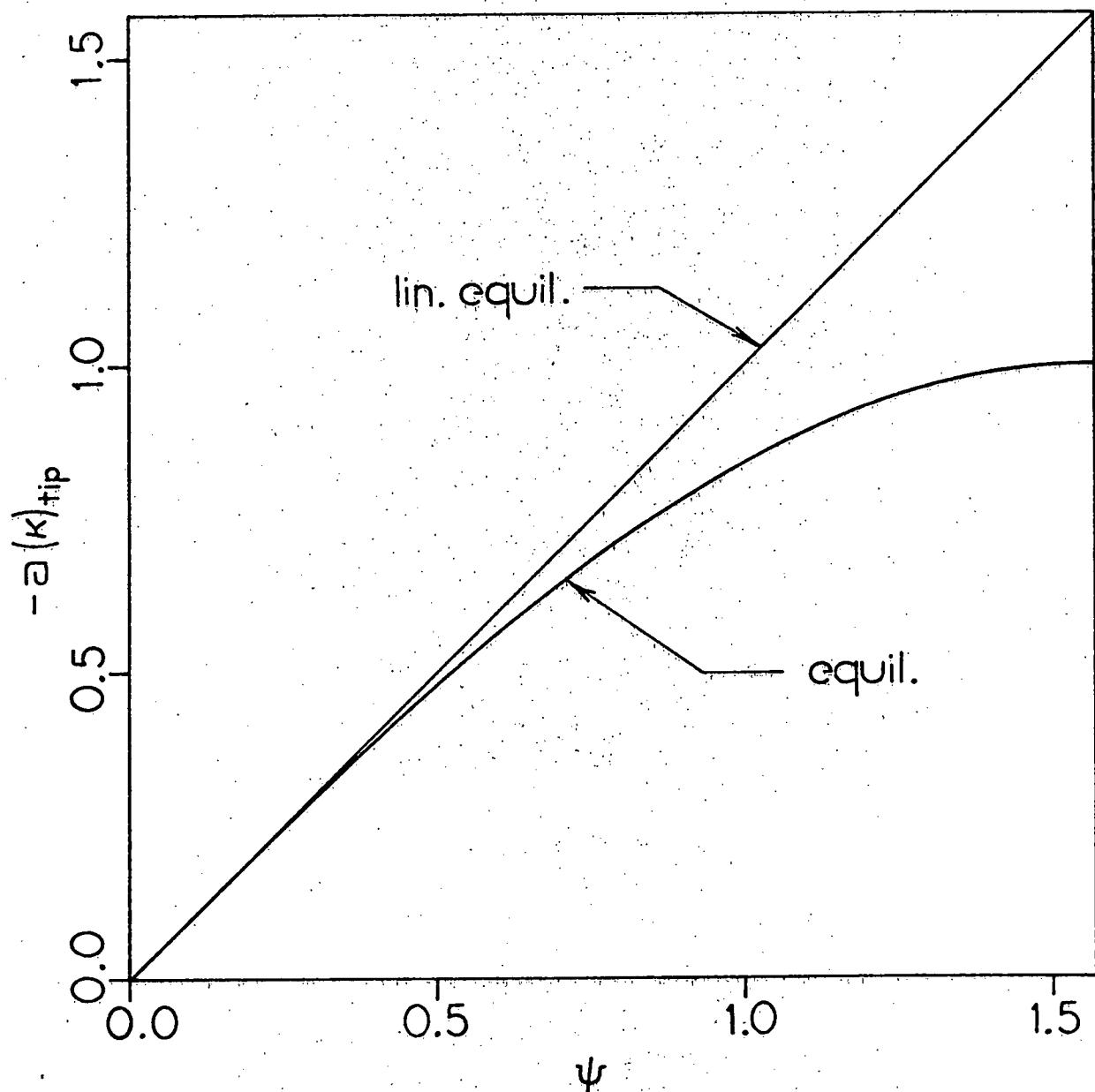
FIGURE 3.2
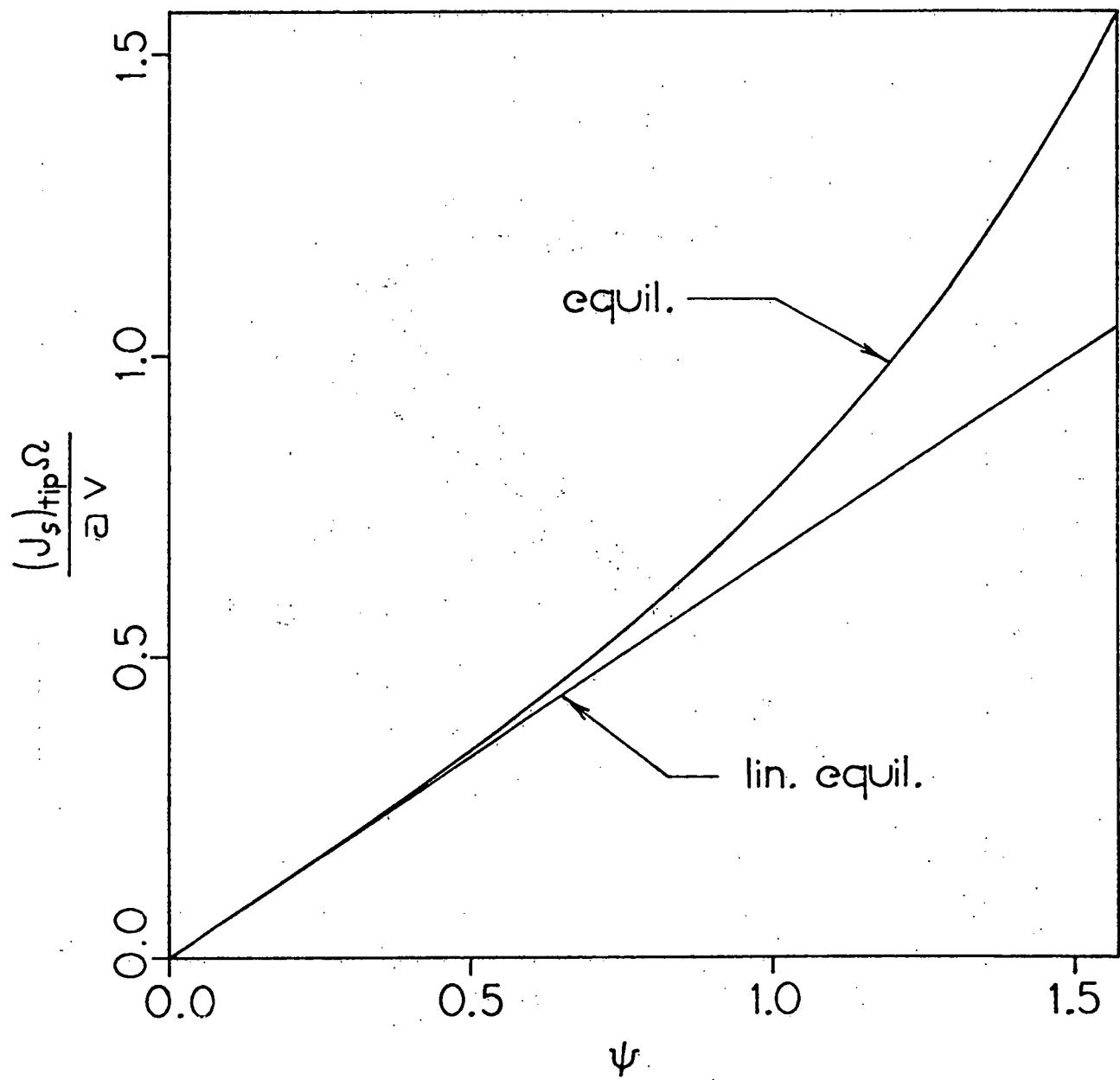
FIGURE 3.3
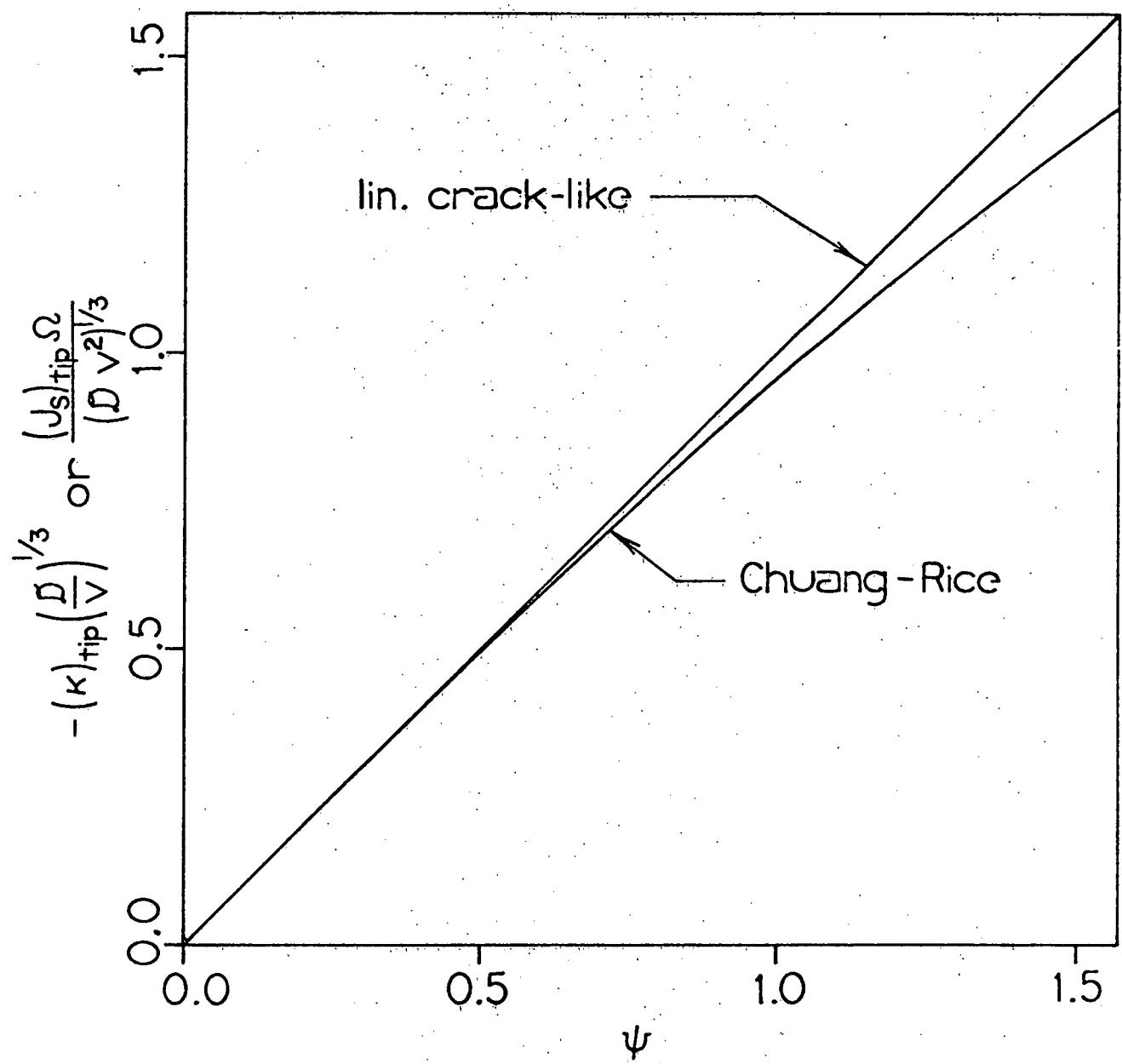
FIGURE 3.4
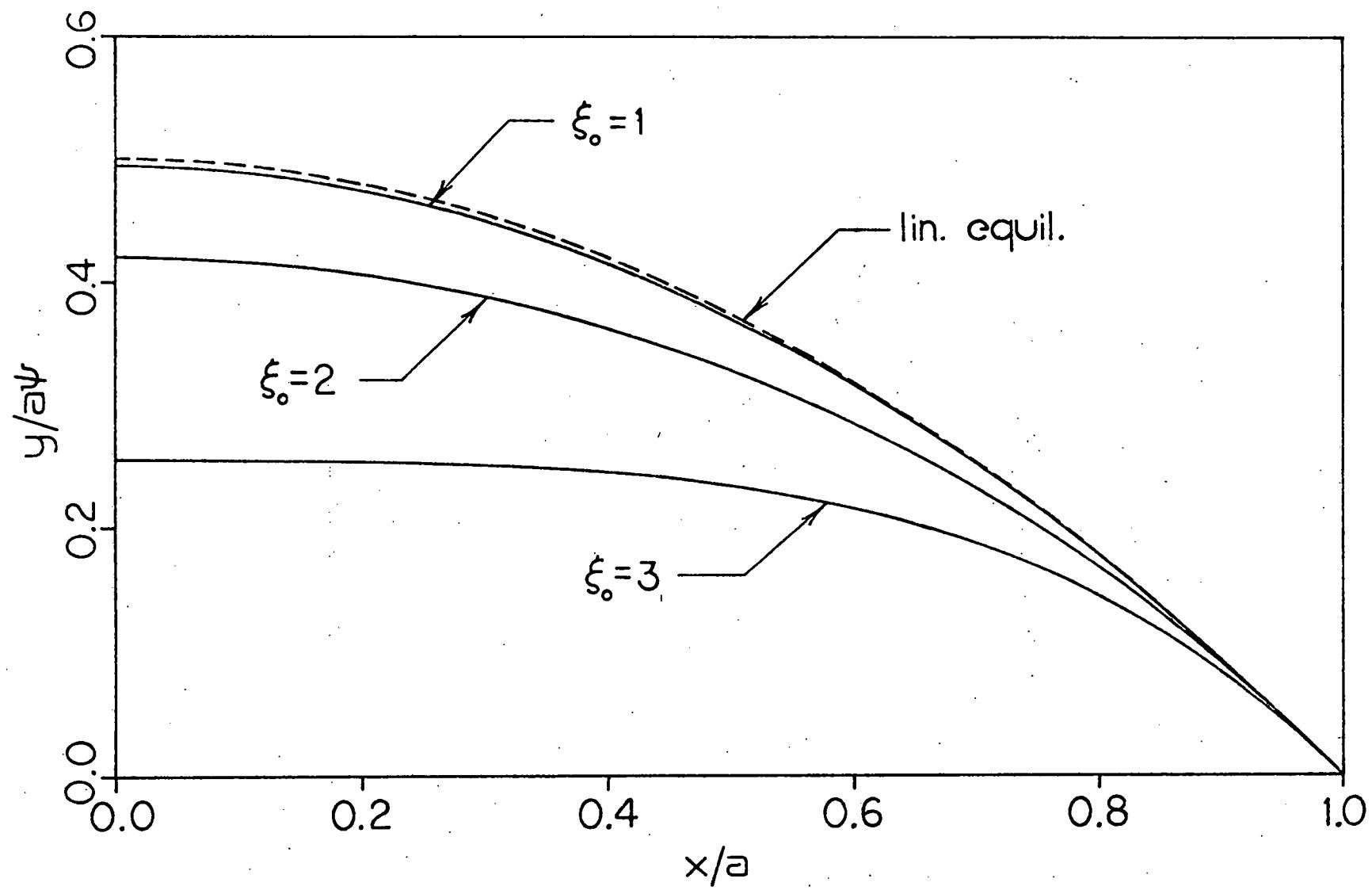
FIGURE 3.5
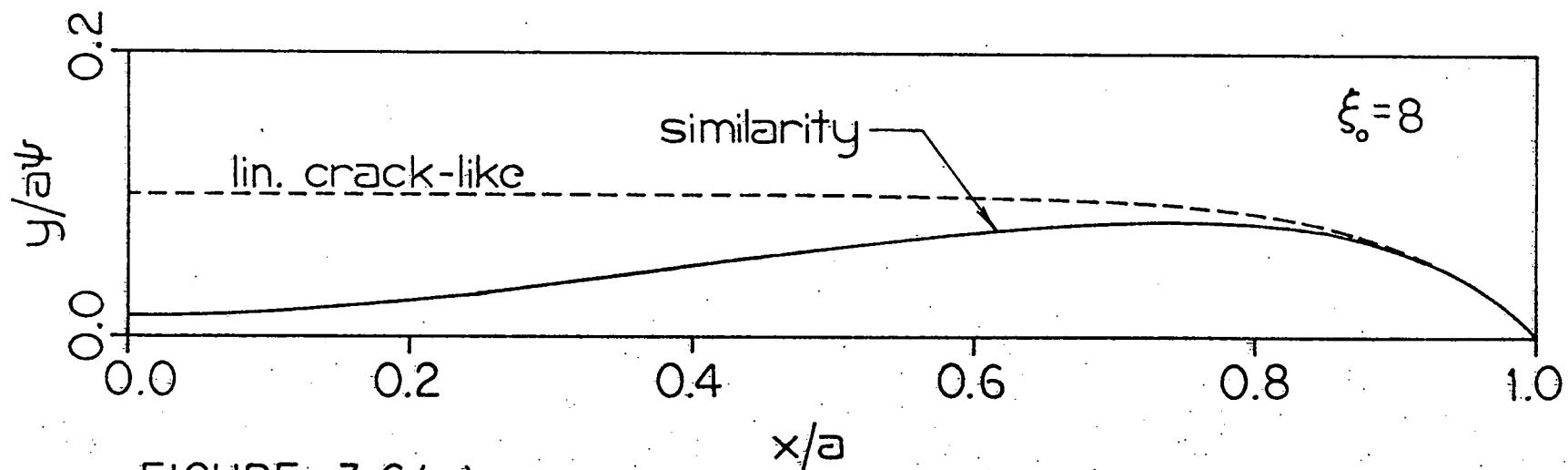
FIGURE 3.6 (a)
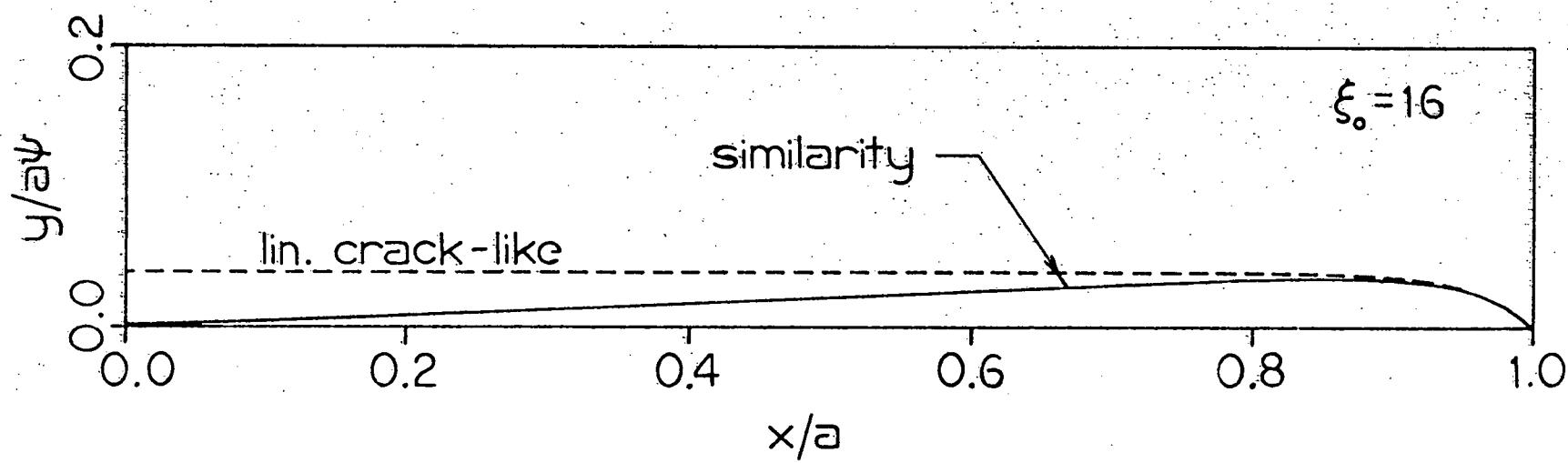
FIGURE 3.6 (b)
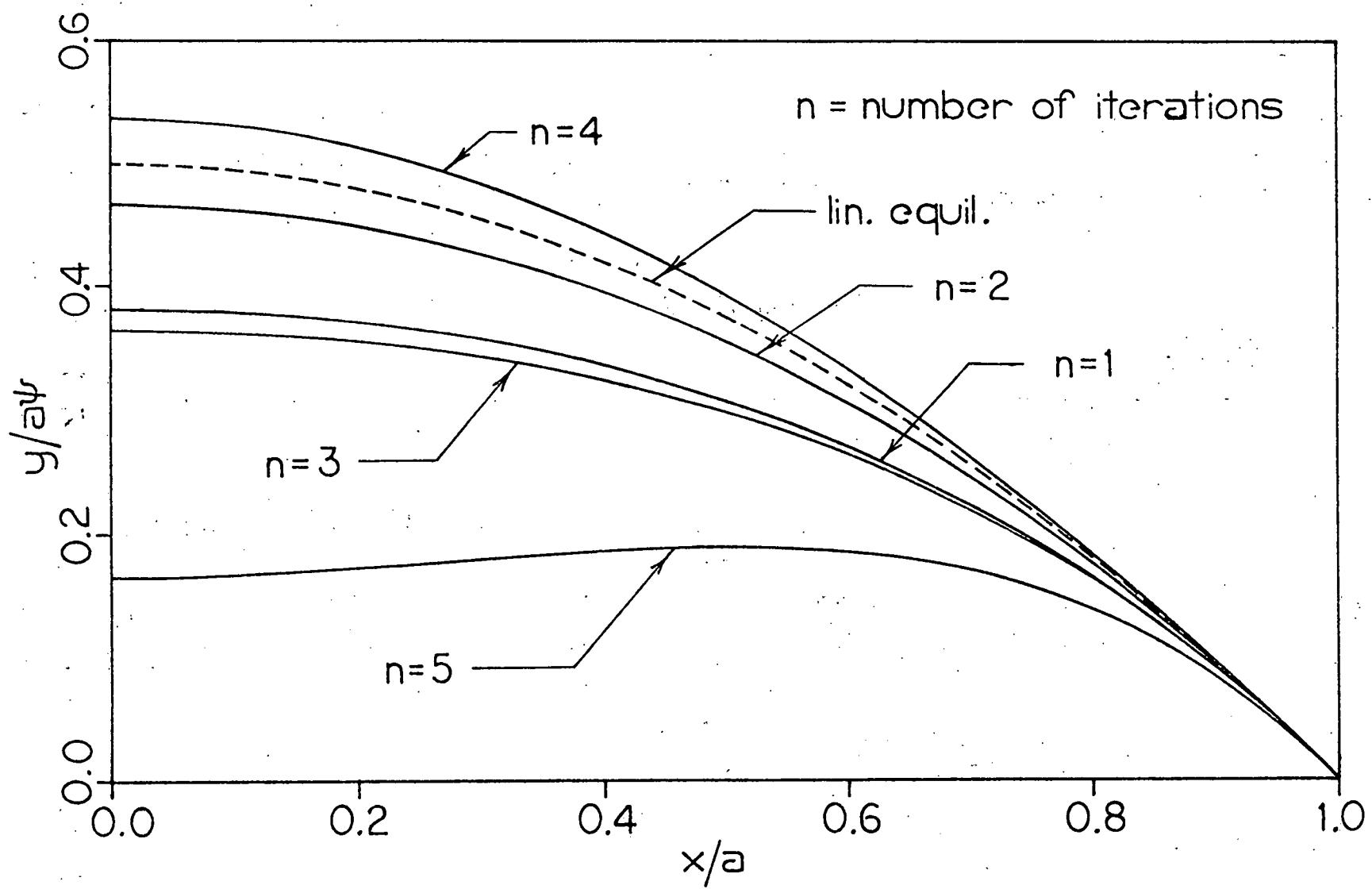
FIGURE 3.7
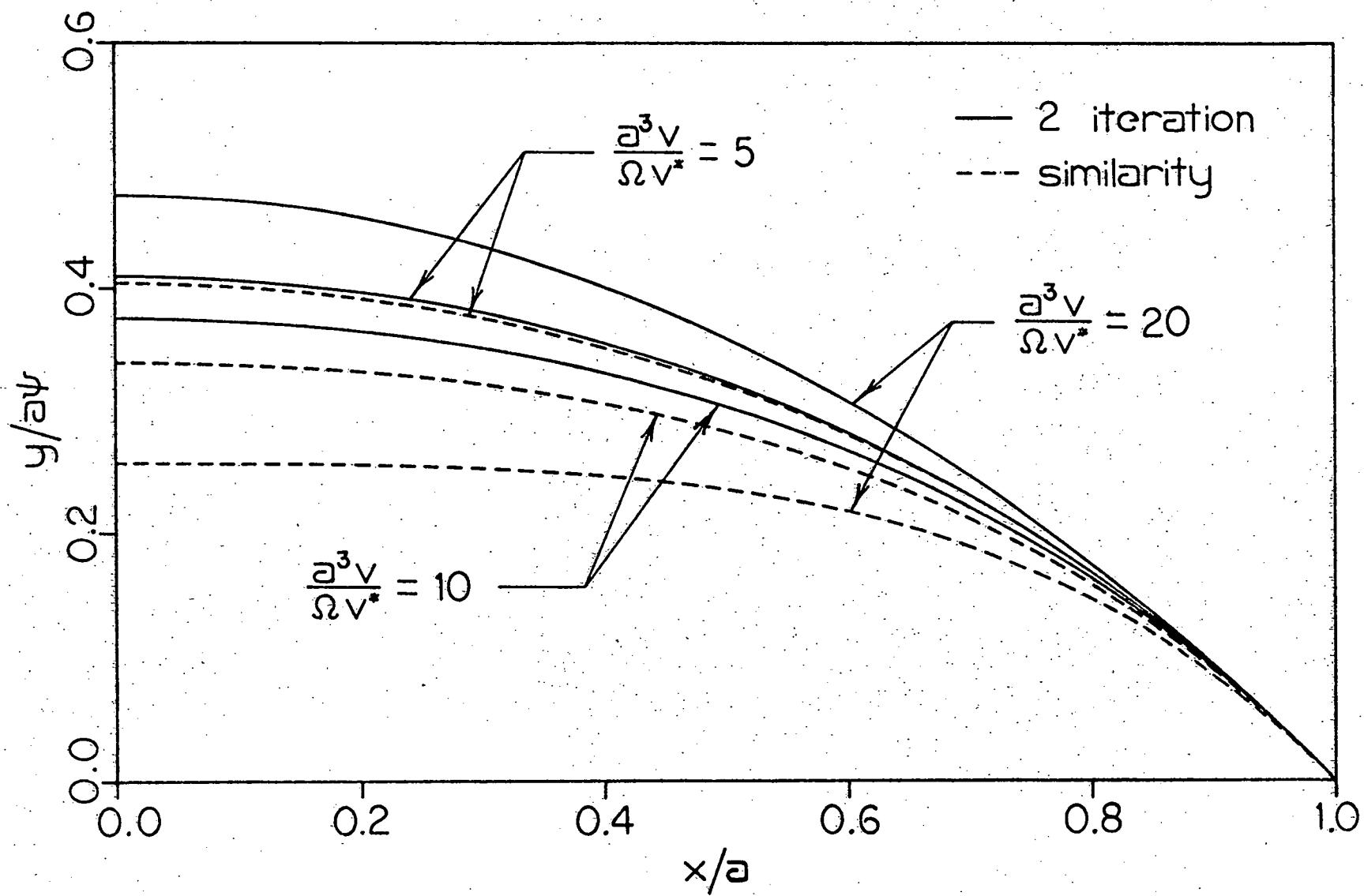
FIGURE 3.8
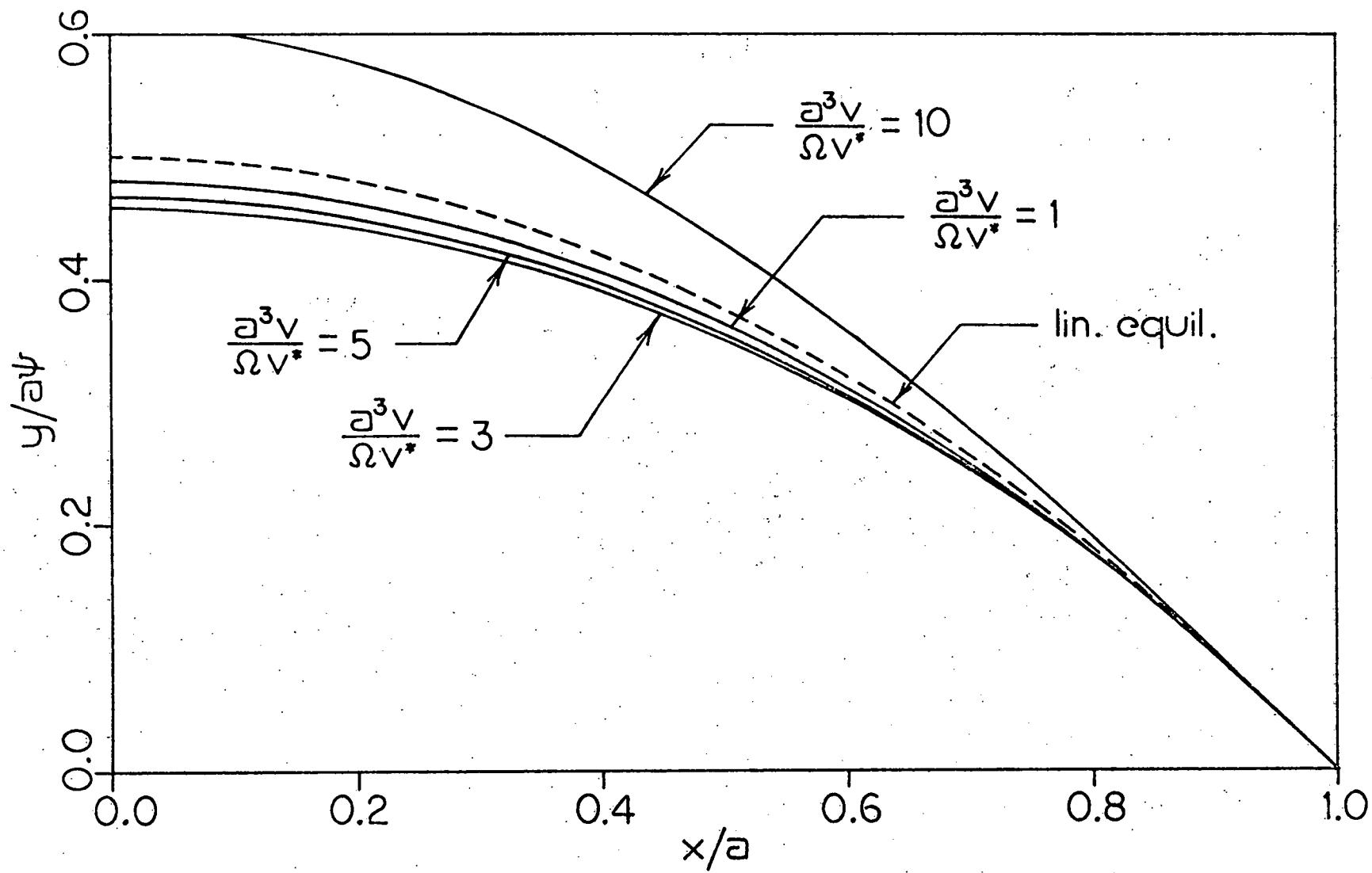
FIGURE 3.9
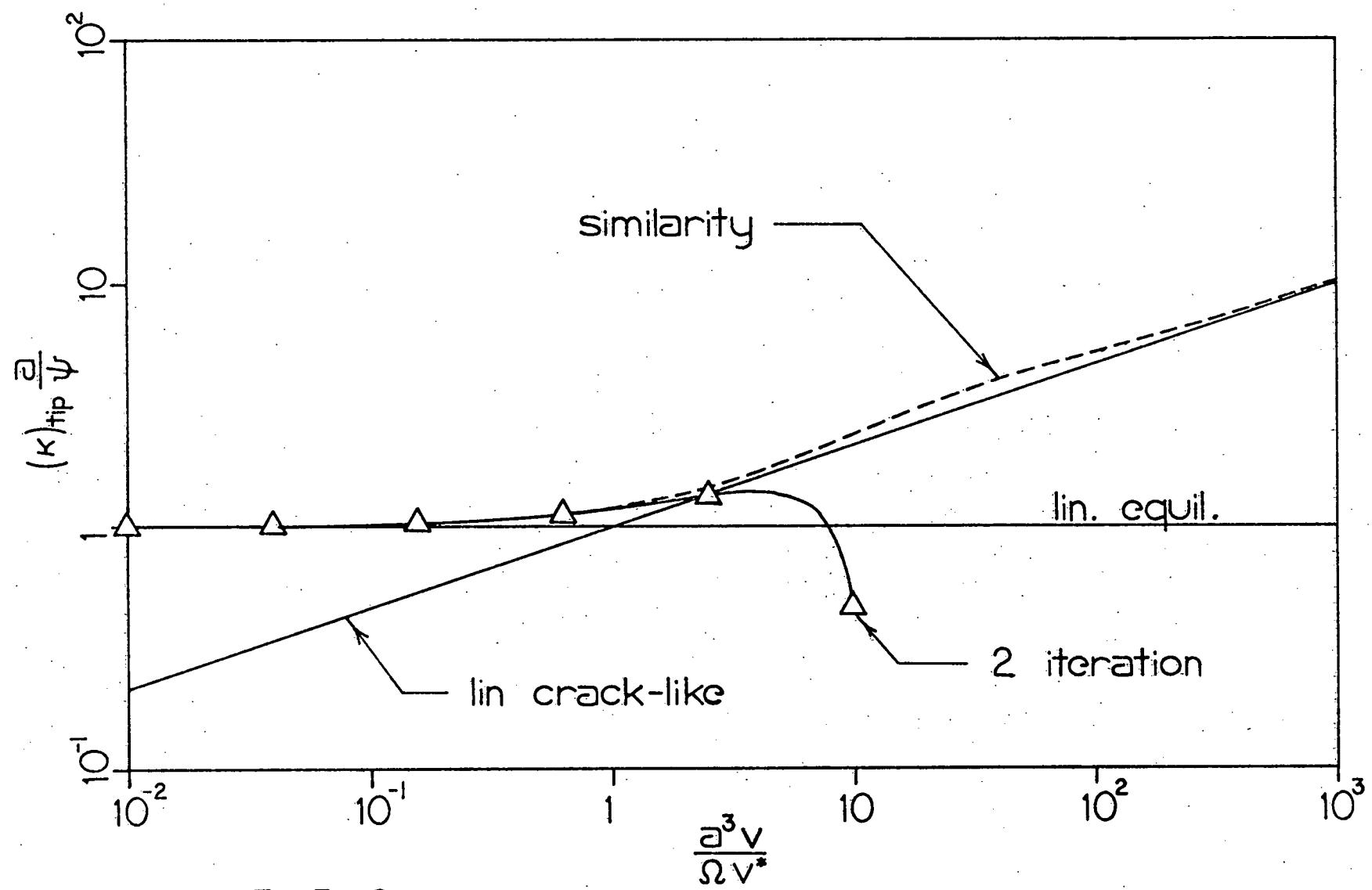
FIGURE 3.10
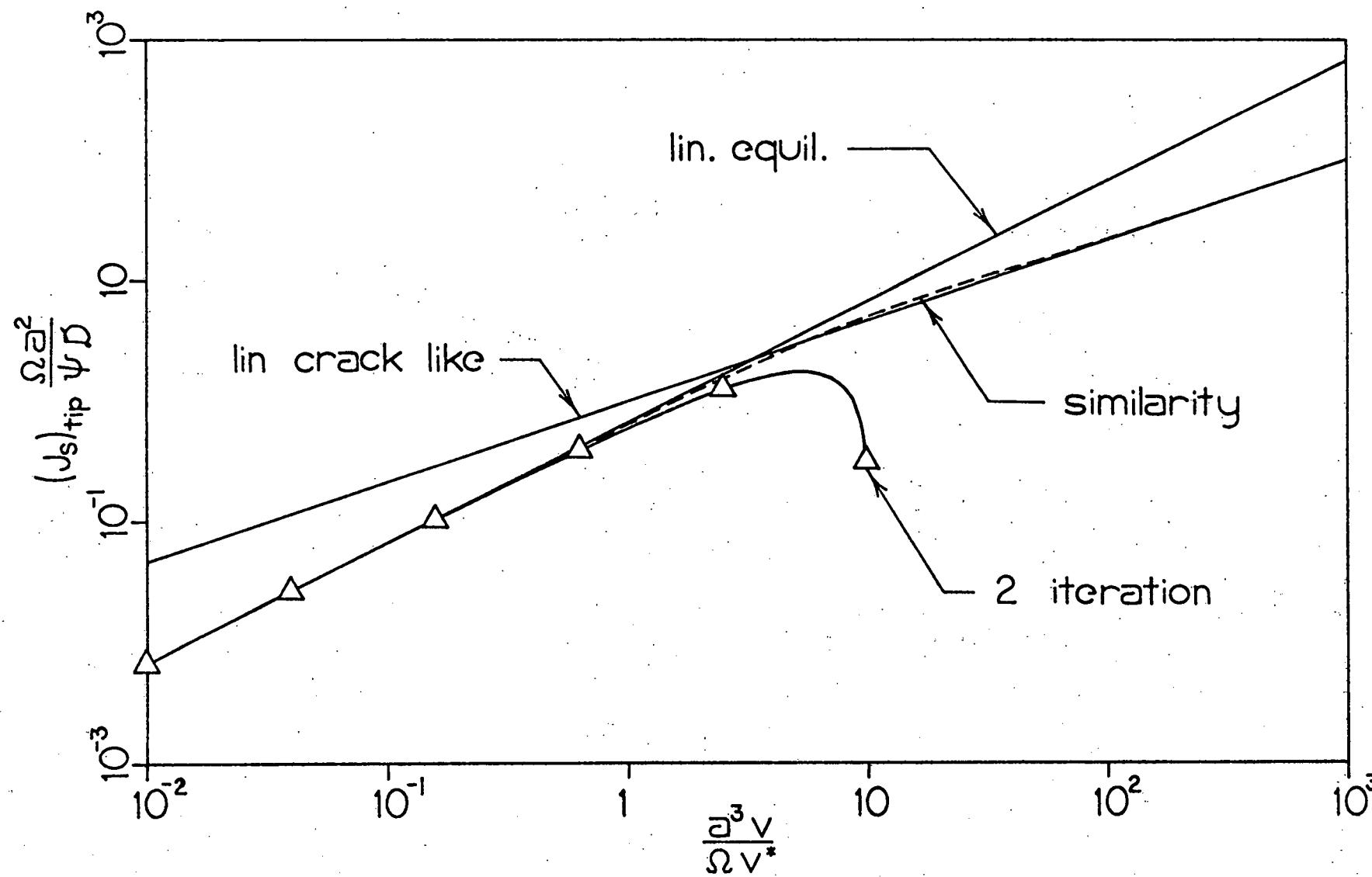
FIGURE 3.11
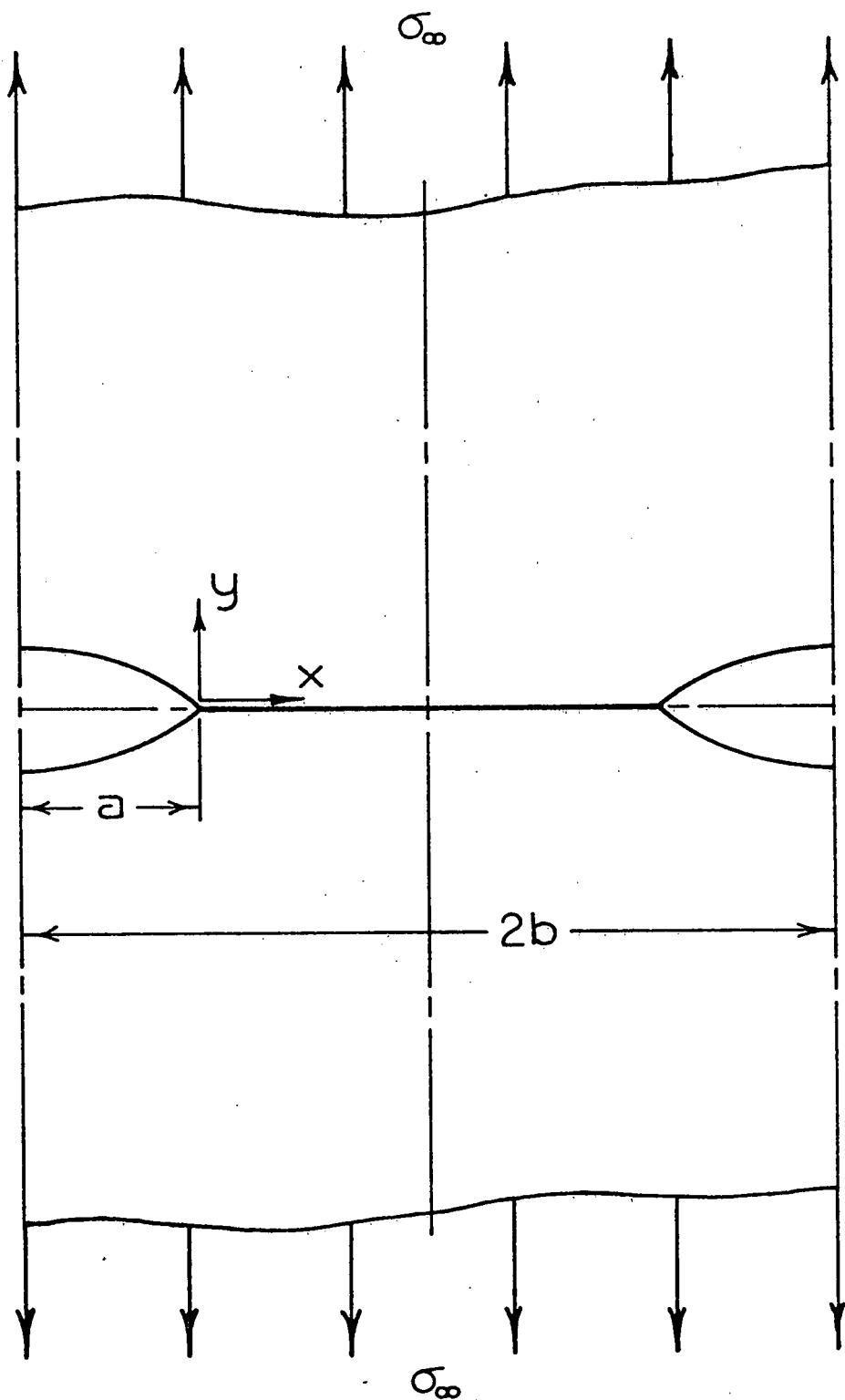
FIGURE 4.1
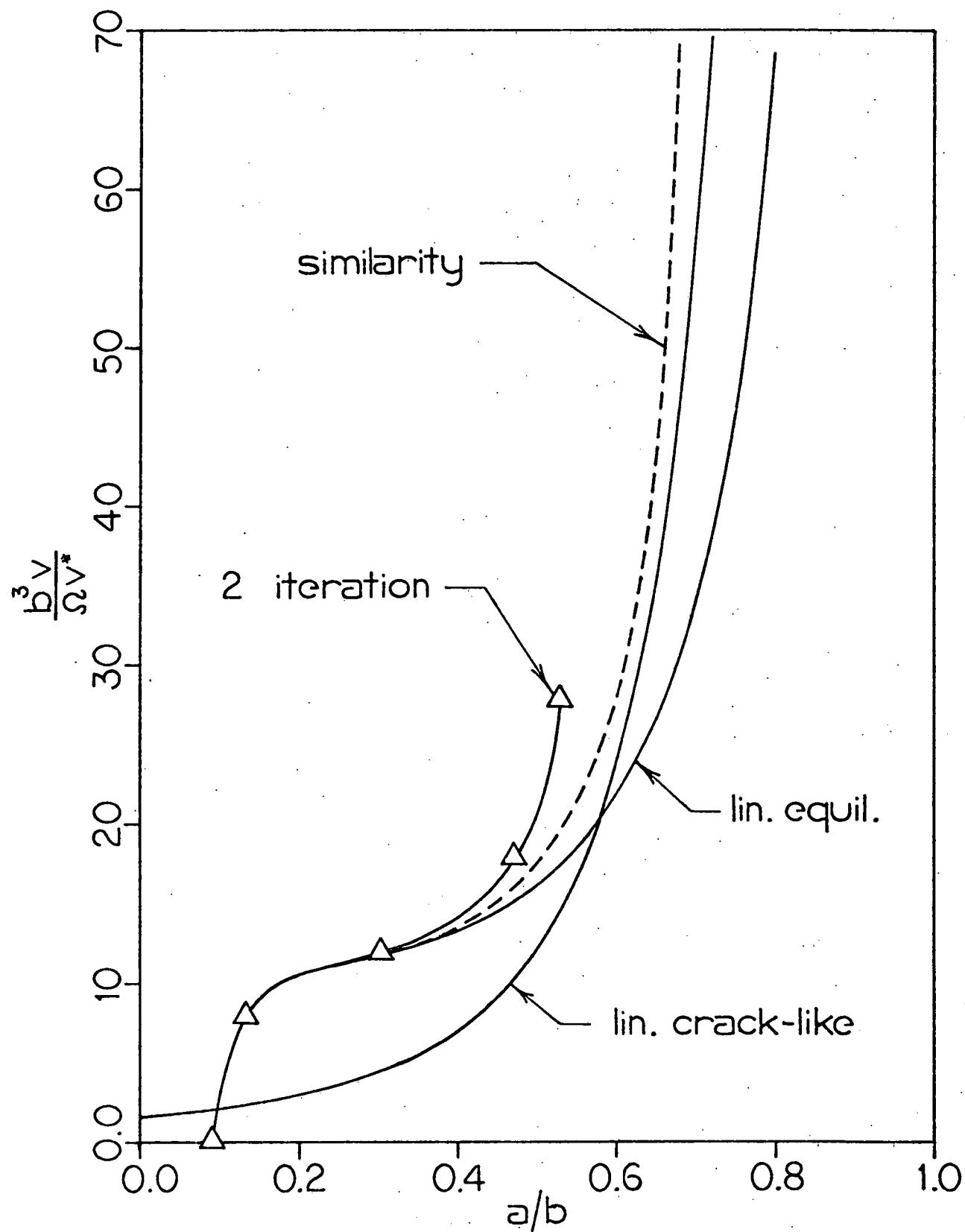
FIGURE 4.2

FIGURE 4.3

FIGURE 4.4